Technical Review

To Advance Techniques in Acoustical, Electrical and Mechanical Measurement

$$a(t) \quad \boxed{1;\ \tau_1} \quad \boxed{2;\ \tau_2} \quad n(t) \quad \Sigma \quad b(t) \quad \boxed{m;\ \tau_m}$$

DUAL CHANNEL FFT ANALYSIS (PART II)

TECHNICAL REVIEW

No. 2 — 1984

Contents

DUAL CHANNEL FFT ANALYSIS (PART II)

by

H. Herlufsen, (M.Sc.)

ABSTRACT

In the first part of this article the basic dual channel FFT measurement was introduced and Frequency Response Function estimates and excitation techniques were discussed.

In the second part of this article the time domain functions, Impulse Response Function, Autocorrelation and Cross Correlation and their physical interpretation is dealt with in some detail. The implementation of the Hilbert Transform on these time domain functions, to compute the corresponding complex analytical signals, is introduced, and the advantages of using the magnitude in the presentation of these functions in some practical situations are illustrated. Calculation of sound intensity from a dual channel measurement of the sound pressure signals from two closely spaced microphones is discussed in terms of advantages and disadvantages.

Formulae for random errors on some of the functions derived from a dual channel measurement on random data are also given.

SOMMAIRE

La première partie de cet article donnait les notions de base des mesures FFT en bi-voie, et discutait des estimations des réponses en frequence et des techniques d'excitation.

Cette deuxième partie traite plus en detail des fonctions du domaine temporel et de réponse impulsionnelle, de l'auto-corrélation, de l'intercorrelation et de leur interpretation physique. Elle introduit aussi l'application de la transformée de Hilbert à ces fonctions temporelles pour calculer les signaux analytiques complexes correspondants, et illustre par quelques cas pratiques les avantages de l'utilisation de l'amplitude pour la representation de ces fonctions. Le calcul de l'intensite acoustique à partir de la mesure bi-voie de la pression sonore de deux microphones rapprochés est traité par comparaison des pours et des contres.

Des formules d'erreurs aléatoires sur quelques unes des mesures en bi-voie sur des données aléatoires sont également données.

ZUSAMMENFASSUNG

Der erste Teil dieses Artikels war eine Einführung in die Zwei-Kanal-FFT-Meßtechnik. Es wurden Übertragungsfunktionsnäherungen und Anregungstechniken diskutiert.

Der zweite Teil beschäftigt sich detailierter mit Zeitbereichsfunktionen, Impulsantwort, Autokorrelation und Kreuzkorrelation sowie ihrer physikalischen Interpretation. Die Anwendung der Hilbert-Transformation auf diese Zeitfunktionen zur Berechnung des komplexen analytischen Signals wird vorgestellt und der Vorteil der Darstellung des Betrags dieser Funktionen wird an einigen praktischen Beispielen illustriert.

Die Vor- und Nachteile der Schallintensitätsmessung mit einem Zweikanalsystem und zwei dicht nebeneinander liegenden Druckmikrofonen wird diskutiert. Zusätzlich werden Formein fur die Berechnung der statistischen Fehler der aus der Messung stochastischer Daten mit dem Zweikanal-System abgeleiteten Funktionen gegeben.

6. Impulse Response Function

The ideal system defined in Section 4 and shown in Fig.14 can be described by its Frequency Response Function $H\{f)$ *as* discussed in Section 4. The corresponding time domain description of the system is given by the Impulse Response Function $h(\tau)$ which can be calculated from the Frequency Response Function by an inverse Fourier Transform.

$$h(\tau) = \mathscr{F}^{-1}\left\{H(f)\right\} = \int_{-\infty}^{\infty} H(f)\, e^{j2\pi f\tau}\, df \qquad (6.1)$$

Physically the Impulse Response Function $h(\tau)$ is the response signal from the system caused by an unit impulse input signal at time 0. Mathematically the unit impulse signal is defined by the socalled Dirac delta function $\delta(t)$ (see Ref. [3] and [4] for instance).

The Dirac delta function $\delta(t)$ is an impulse at $t = 0,$ which is infinitely short in time and infinitely high in amplitude, such that its time integral is unity, i.e.:

$$\int_{-\infty}^{\infty} \delta(t)\, dt = 1$$

The Fourier transform of $\delta(t)$ is unity at all frequencies i.e.

$$F\left\{\,\delta(t)\,\right\} = 1, \qquad -\infty < f < \infty$$

which means that all frequencies are excited to the same level if an input signal of a (t) = $\delta(t)$ is applied to the system.

4

According to eq. (1.2) (Part I of this article) we therefore have $B(f)$ = $H(f)$, since $A(f) = 1$ for $a(t) = h(t)$. Thus

$$B(t) = F^{-1}\{ H(f) \} = h(t) \text{ for a(t)} = \delta(t) \qquad (6.2)$$

Let us now consider a general input signal a(t) to the system and find the output signal $b(t)$ from a time domain description. Any time signal a(t) can be written as a sum of weighted and time shifted delta functions i.e.:

$$a(t) = \int_{-\infty}^{\infty} a(\tau)\, \delta(t-\tau)\, d\tau$$

Each of these weighted and time shifted delta functions a(τ) δ(t-τ) at the input will at the output give a signal which is the Impulse Response Function, weighted with a(τ) and shifted τ in time i.e.: a(τ) $h(t - \tau)$. The output signal $b(t)$ from the system, when excited with a(t) at the input, is therefore the superposition of these weighted and time shifted Impulse Response Functions, assuming linearity, giving:

$$b(t) = \int_{\infty}^{\infty} a(\tau)\, h(t-\tau)\, d\tau \; = \; a(t) \, \bigstar \, h(t) \qquad (6.3)$$

$b(t)$ is said to be the convolution of $a(t)$ and $h(t)$. Since $a(t) * h(t)$ = $h(t) * $a(t), eq.(6.3) is the same as eq. (1.1) (Part I of the article).

It can also be said that eq. (6.3) (or eq.(1.1)) is a direct consequence of the relation: $B(f)$ = $H(f)$ · $A(f)$ (eq.(1.2)) and the Convolution Theorem for the Fourier Transform, which states that multiplication in one domain (here frequency domain) corresponds to convolution in the other domain (the time domain).

From equation (6.3) we can see that $h(\tau)$ acts as a "memory function" of the system. The output $b(t_o)$ at time to not only depends upon the input value at time t_o, $a(t_o)$, but also depends upon the previous values in $a(t)$ weighted with the reversed Impulse Response Function $h(t_o - t)$.

Let us first consider a single degree of freedom system shown in Fig.35, which consists of a mass m supported by a spring, with a spring constant k, and a viscous damper with damping coefficient c. The mass is allowed to move in only one direction x. The input could be the force acting on the mass $f(t)$, while the output could be the displacement $x(t)$. The force caused by the spring is $-kx(t)$ and the damping force is $-cx(t)$, where x(t) is the velocity (time derivative of $x(t)$).
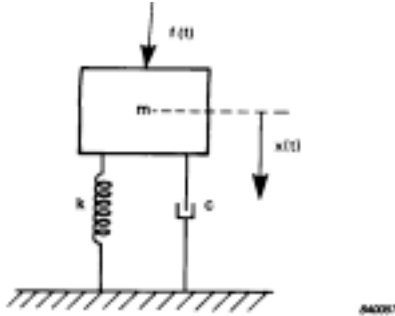
Fig. 35. Mechanical single degree of freedom system

Having the force as the input and the displacement as the output, the Frequency Response Function of the system is the socalled compliance. It is for this simple system given by:

$$H(\omega) = \frac{X(\omega)}{F(\omega)} = \frac{1/m}{-\omega^2 + j\omega\,\dfrac{c}{m} + \dfrac{k}{m}}$$

$$= \frac{A}{j\omega - (j\omega_d - \sigma)} + \frac{A^*}{j\omega - (-j\omega_d - \sigma)} \qquad (6.4)$$

where $\omega = 2\pi f$ and $X(\omega)$ and $F(\omega)$ are the Fourier Transforms of $x(t)$ and $f(t)$ respectively.

A is a constant and mathematically called the residue for the resonance. It is here imaginary and given by

$$A = -\frac{1}{j2m\omega_d} \qquad (6.5)$$

In the literature the residue is sometimes defined by $R = j2A$, which is real valued, and (6.4) becomes

$$H(\omega) = \frac{R}{j2\,[j\omega - (j\omega_d - \sigma)]} - \frac{R}{j2\,[j\omega - (-j\omega - (j\omega_d - \sigma)]} \qquad (6.6)$$

The constants ω_d and σ are given by $\quad \omega_d = \sqrt{\dfrac{k}{m} - \dfrac{c^2}{4m^2}} \qquad (6.7)$

and $\qquad \sigma = \dfrac{c}{2m} \qquad (6.8)$

6

The corresponding Impulse Response Function $h(t)$ is found by an inverse Fourier Transform of (6.4) or (6.6) and is given by

$$h(t) = 2 \mid A \mid e^{-\sigma t} \sin (\omega_d t) \tag{6.9}$$

or
$$h(t) = R\, e^{-\sigma t} \sin (\omega_d t) \tag{6.10}$$

Fig.36 shows an example of log $\mid H(f) \mid$ and phase $\Phi(f)$ of $H(f)$ and the corresponding $h(t)$ for the single degree of freedom system.

ω_d is called the damped natural frequency and is the frequency (in radians per second) of the oscillations in $h(t)$ (see Fig.36). σ is the decay rate determining the exponential decay of $h(t)$, shown as the dotted envelope curve in Fig.36 (lower graph).

Notice that the higher the damping is in the system the faster is the decay of the Impulse Response Function $h(t)$ and the shorter will the effective length of $h(t)$ be.

The socalled undamped natural frequency ω_0 is defined by

$$\omega_0 = \sqrt{\omega^2_d + \sigma^2} = \sqrt{\frac{k}{m}} \tag{6.11}$$

If the system had no damping i.e. $c = 0$, the mass would be oscillating at a frequency of coo after an initial impulse excitation.

The damping is also often given by the damping ratio ζ which is defined by

$$\zeta = \frac{\sigma}{\omega_0} \tag{6.12}$$

For $\zeta = 1$ the system is said to be critically damped since in that situation $\omega_d = 0$ and there will be no oscillations in $h(t)$.

The Impulse Response Function can thus be used for determination of the damped natural frequency ω_d, the decay rate σ and the constant A (or R) for a single degree of freedom system. A practical example of determination of decay rate σ will be given later.

In some acoustical and electroacoustical applications, where an input can be defined and measured, the Impulse Response Function is used
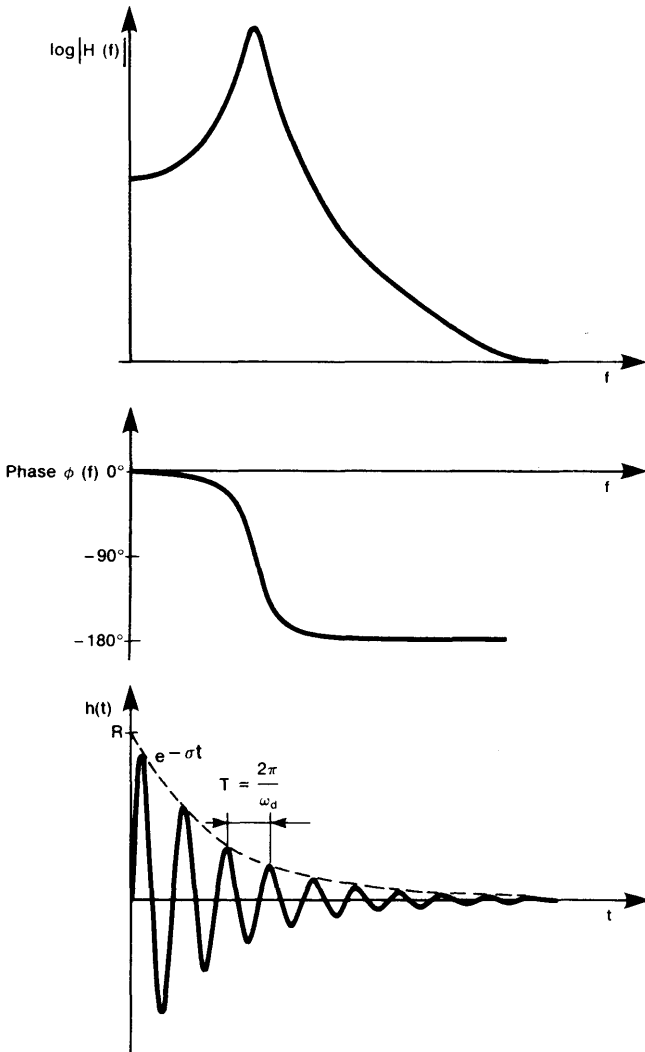
Fig. 36. Logarithmic amplitude log |H(f)| and phase φ(f) of the Fre-
quency Response Function and corresponding Impulse Response
Function of a single degree of freedom system

for determination and recognition of reflections, their time delays and
individual magnitudes. For non-dispersive media where no filtering oc-

curs in the frequency band of interest, reflections will show up as narrow peaks in the Impulse Response Function at the points in time corresponding to the delay times. The Impulse Response Function can therefore also be used for identification of transmission paths   This technique has some advantages compared to the use of Cross Correlation Function, which is discussed in Section 7. Since the Impulse Response Function describes the system independent of the signals involved, the propagation paths can be recognized even though the input signal is shaped in frequency by some filtering. Filtering of the signals will cause the Cross Correlation Function to be smeared and can therfore make the transmission paths identification difficult. This will be illustrated in Section 7. In order to be able to calculate the Impulse Response Function, however, there has to be some input signal at all the frequencies of consideration, since the Frequency Response Function will be undefined at those frequencies where no input signal exists.

Traditionally the Impulse Response Function hasn't been used very much compared to the Frequency Response Function. $h(t)$ is a real valued function and is presented on a linear amplitude scale. The dynamic range of a linear presentation is very limited and oscillations in $h(t)$ due to filtering of the signal in the system often complicates the interpretation of the results.

With the implementation of the Hilbert Transform in the time domain, all the time domain functions including the Impulse Response Function can be made analytical (complex), i.e. they will have a real and an imaginary part. They can therefore be presented in terms of magnitude and phase as well. The Hilbert Transform, which is defined as a convolution integral, is used to compute the imaginary part $j\tilde{a}(t)$ of the analytical signal from the real valued time signal a(t). It is denoted by H and we have

$$\tilde{a}(t) = \mathscr{H}\left\{a(t)\right\} = \int_{-\infty}^{\infty} a(\tau)\frac{1}{\pi(t-\tau)}\,d\tau \tag{6.13}$$

and the socalled analytical time signal $\breve{a}(t)$ is then defined as

$$\breve{a}(t) = a(t) + j\tilde{a}(t) \tag{6.14}$$

The theory behind the Hilbert Transform is defined and discussed in Ref. [12] and [13]. It is found that the Hilbert Transform of a time function can be computed much simpler in the frequency domain compared to a direct calculation in the time domain. The spectrum of the time signal a(t) is shifted -90° for positive frequencies and +90° for negative

9

frequencies. An inverse Fourier Transform of this modified spectrum will result in the time signal a(f), which Is the Hllbert Transform of a(t). This technique is used in the B&K Analyzers Type 2032/2034.

Having the complex (analytical) Impulse Response Function

$$\breve{h}(t) = h(t) + j\tilde{h}(t) \tag{6.15}$$

the magnitude is defined as

$$|\breve{h}(t)| = \sqrt{h^2(t) + \tilde{h}^2(t)} \tag{6.16}$$

while the phase is given by

$$\theta_h(t) = \text{Arctan} \left(\frac{\tilde{h}(t)}{h(t)} \right) \tag{6.17}$$

The magnitude $|\breve{h}(t)|$ can be considered as being the envelope of $h(t)$ and this presentation is often much more useful than just the real valued $h(t)$. Firstly, the magnitude does not feature the oscillations often seen in $h(t)$, but gives a smooth curve where identification of reflections, for instance, is much easier and where the peak amplitudes will be correct and consistent. Secondly, the magnitude can be shown on a logarithmic amplitude scale giving more dynamic range in the presentation of the data compared to the conventional linear scale. Fig.37 illustrates this for an acoustical system, where both the input and the output is measured by use of microphones. The Impulse Response Function in this and all the subsequent examples is computed as an inverse Fourier Transform of the Frequency Response Function estimate $H_1(f)$ (see Section 4, Part I of this article). In the upper graph the real valued $h(t)$ is shown, while the lower graph shows the magnitude of the complex $\breve{h}(t)$ with a logarithmic amplitude scale. The magnitude of $\breve{h}(t)$ reveals more details in the Impulse Response Function, and the correct levels and time delays for the different reflections are easily found from the magnitude curve.

In this example the input spectrum is band limited but the Impulse Response Function still detects the different reflections as narrow peaks at the different time delays. The Cross Correlation Function for the same signals does not resolve the reflections as clearly as the Impulse Response Function, due to the frequency band limitation. The Cross Correlation Function for the same signals will be shown in Section 7, (Fig.47).
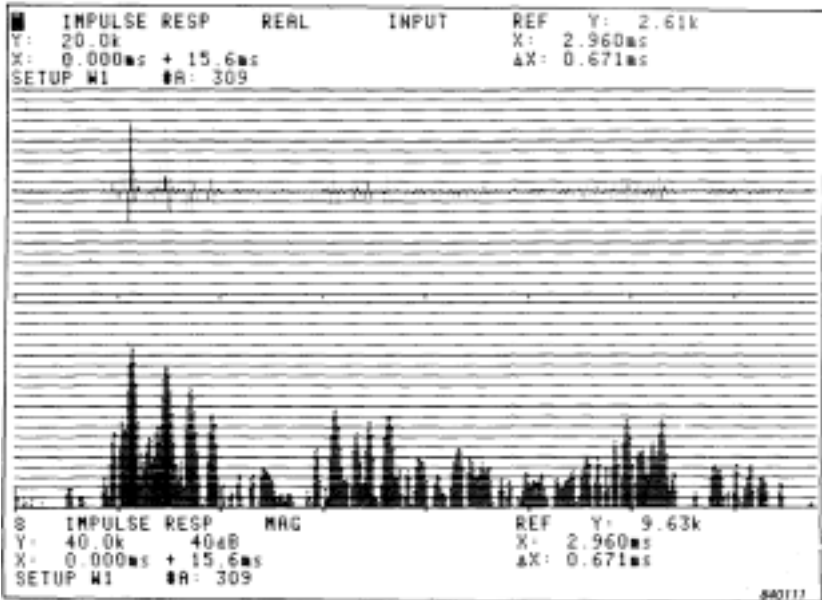
*Fig. 37. Impulse Response Function of an acoustical system. In the upper
graph the real valued h(t) is shown. In the lower graph the
magnitude of the complex Impulse Response Function h(t) is
plotted on a logarithmic amplitude scale*

Computation of the magnitude of the Impulse Response Function was
implemented already several years ago by use of Time Delay Spectrom-
etry (TDS). The magnitude of $\hat{h}(t)$ is then often referred to as the Energy
Time Curve (ETC). For many acoustical and electroacoustical applica-
tions the ETC created new interest and possibilities for the time (delay)
domain description of systems (Ref. [13]).

Let us return to the application of the Impulse Response Function for
determination of damping, given by the exponential decay in *h(t)* (6.9)
for a single degree of freedom system. When a measurement is per-
formed over a frequency range where the system has several reso-
nances, the Impulse Response Function will be complicated and more
difficult to interpret.

Assuming that the system is linear, it can be considered as a combina-
tion of single degree of freedom systems (Fig.35) and is called a multi

degree of freedom system. The Frequency Response Function is there-
fore a linear combination of single degree of freedom Frequency Re-
sponse Functions of the form (6.4), shown in Fig.36. Each resonance is
described by the resonance frequency ω_d, the decay rate σ and the
constant A (or R) called the residue.

The Impulse Response Function will be the corresponding linear combi-
nation of single degree of freedom Impulse Response Functions of the
form (6.9), shown in Fig.36 (lower graph), and can therefore be written as

$$h(t) = \sum_r 2\,|A_r|\; e^{-\sigma_r t}\, \sin\left(\omega_{dr} t\right) \tag{6.18}$$

or
$$h(t) = \sum_r R_r\; e^{-\sigma_r t}\, \sin\left(\omega_{dr} t\right) \tag{6.19}$$

where r is the resonance number (mode number).


```
5    FREQ RESP H1     MAG              MAIN  Y:   32.6dB
Y:   50.0dB    80dB                    X:    █████
X:   0Hz + 3.2kHz     LIN
SETUP W2     #A: 30                    ELEM #: 211
```

```
5    FREQ RESP H1     MAG              MAIN  Y:   32.6dB
Y:   50.0dB    80dB                    X:    844Hz
X:   0Hz + 3.2kHz     LIN
SETUP W2     #A: 30
```
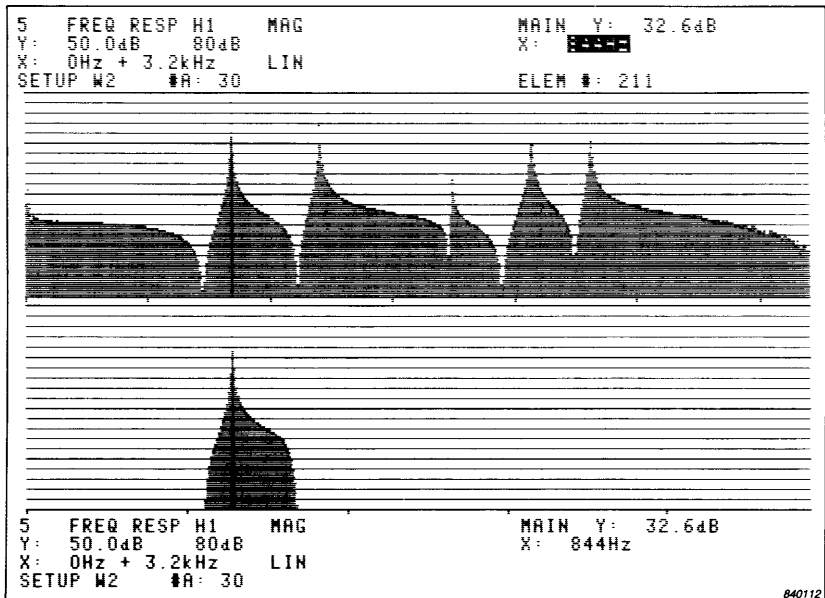
840112

Fig. 38. *Frequency Response Function (driving point acceleration of a
mechanical system) revealing five resonances (upper graph).
Pseudo-random force excitation is used. In the lower graph the
first resonance is extracted by use of the weighting function
shown in Fig.39.*

If the different resonances are well separated in frequency, and the system is lightly damped, each resonance can be treated separately after the measurement, by application of a weighting function on the Frequency Response Function as exemplified in Fig.38. The Frequency Response Function ($H_1(f)$) is here the driving point acceleration for a plate and is measured using shaker excitation. The shaker is attached to the structure via a force transducer and a push rod as shown in Fig.23 (Section 5, Part I of the article). A pseudo-random excitation signal is used in order to avoid leakage in the analysis (see Section 4.6). The system is almost linear and the calculated Frequency Response Function in Fig.38 (upper graph) is therefore samples at $f = k \cdot \Delta f = k \cdot {}^{1}/T$ of the true Frequency Response Function.

In the lower graph of Fig.38 the first resonance (first mode of vibration) at 844 Hz ($\omega_o \cong \omega_d$ = 5303rad/s) is extracted by application of a rectangular weighting function, the position and width of which being defined by the user. Some tapering (half-Hanning) is applied in the beginning and at the end of the rectangular weighting in order to avoid sharp edges (truncation) in the edited Frequency Response Function. The weighting function applied in Fig.38 is shown in Fig.39.
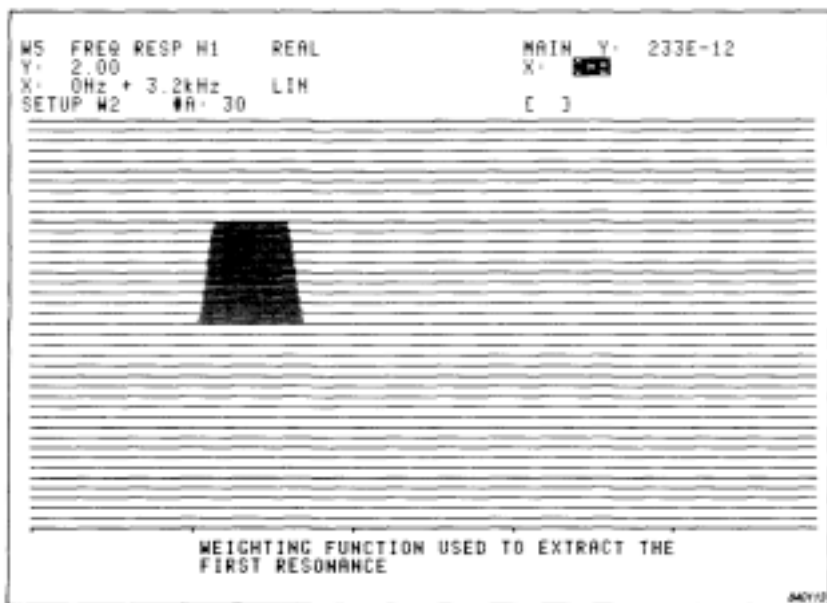

Fig. 39. *The user defined weighting function used for extracting the first resonance, as shown in Fig.38.*

```
7   IMPULSE RESP    REAL              MAIN  Y:   313
Y:  1.50k                             X:  ▮▮▮▮▮▮▮
X:  0.00ms + 125ms
SETUP W2    #A: 30                    [   ]
```

```
8   IMPULSE RESP    MAG               REF   Y:  52.2dB
Y:  80.0dB    40dB                    X:   111.20ms
X:  0.00ms + 125ms                    ΔX:  103.63ms
SETUP W2    #A: 30                    ΔY   : -8.7dB
```
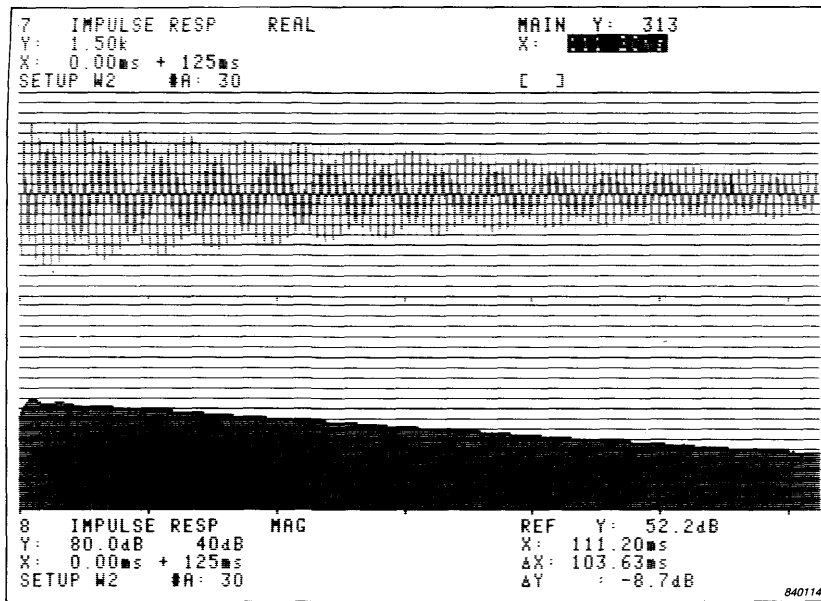
Fig. 40. Real valued Impulse Response Function h(t) (upper graph) and magnitude of complex Impulse Response Function #(t), shown on a logarithmic amplitude scale (lower graph), for the first resonance

An inverse Fourier Transform of the edited Frequency Response Function ($H_1(f)$) in the lower graph of Fig.38 results in the Impulse Response Function of this single resonance (first mode of vibration) and is shown in Fig.40 (upper graph). The magnitude of the corresponding complex (analytical) Impulse Response Function, (6.15) and (6.16), is computed and shown in the lower graph of Fig.40, with a logarithmic amplitude scale. The exponential envelope curve $e^{-\sigma\,t}$, determined by the decay rate σ, can now be seen as a linear decay. The time constant τ of the exponential decay is given by $\tau = {}^1/\sigma$. The decay corresponding to the time constant τ is given by the factor e^{-1} or in dB: $-20\log(e) = -8,7$ dB.

By use of the reference cursor the time constant τ can be found directly and is for this resonance $\tau_1 = 103,6$ms, as seen from the Δx readout in the lower right corner of Fig.40. The decay rate for this resonance is therefore

14

$$\sigma_1 = \frac{1}{\tau_1} = 9,65 \text{ rad/s}$$

and the damping ratio is $\quad \zeta_1 = \frac{\sigma_1}{\omega_{01}} = 0,0018$.

In a similar manner the other resonances can be extracted from the same measurement and the decay rate of these can be found. In Fig.41, the second resonance (second mode of vibration) and the fifth resonance (fifth mode of vibration) are extracted using the same kind of weighting function as the one shown in Fig.39 shifted to the relevant resonance.

The magnitude of the corresponding Impulse Response Functions on logarithmic amplitude scales are shown below the respective edited Frequency Response Functions. The time constants τ_2 and τ_5 are found to be τ_2= 92,0 ms and τ_5 = 48,9 ms (see Δx in the cursor read outs). This corresponds to decay rates of
σ_2 = 10,9 rad/s and σ_5 = 20,4rad/s respectively.

The undamped natural frequency ω_{0r}, on is approximately equal to the damped natural frequency ω_{dr}, since the damping is light and is 1204 Hz and 2312 Hz (i.e. 7565 rad/s and 14527 rad/s) for the two resonances. This gives damping ratios of ζ_2 = 0,0014 and ζ_5 = 0,0014 respectively.

The decay rate for a resonance can also be determined from the half power (3dB) bandwidth $\Delta f = \frac{\Delta \omega}{2\pi}$ of the resonance peak in the Frequency Response Function, assuming that the resonance is well separated from other resonances. In this case σ is given by $\sigma = \pi f$ or in terms of damping ratio $\zeta = \frac{\pi \Delta f}{\omega_0} = \frac{\Delta f}{2f_0}$ For lightly damped structures it is necessary to use a frequency resolution which is high in order to find the half power bandwidth of the resonances. Zoom analysis will therefore often be required and several measurements must be performed in order to cover the frequency range of interest. Using the Impulse Response Function calculation in combination with the editing technique as shown, only one baseband measurement is required in order to find the decay rate (or damping ratio) for the different resonances. Notice however that pseudo-random excitation has to be used in order to avoid leakage. Leakage will have the effect of broadening out the resonance peak (see Fig.10) and the estimated decay rate will therefore be wrong (too high), at least when $H_1(f)$ is used for calculation of the Impulse Response Function.

```
5    FREQ RESP H1      MAG                    MAIN  Y:  -147.5dB
Y:    50.0dB      80dB                        X:   3200Hz
X:    0Hz + 3.2kHz      LIN
SETUP W2      #A: 30
```

```
8    IMPULSE RESP      MAG                    REF    Y:   55.5dB
Y:    80.0dB      40dB                        X:   ▓▓▓▓▓
X:    0.00ms + 125ms                          ΔX:  92.04ms
SETUP W2      #A: 30                a)         ΔY     : -8.7dB        840115
```

```
5    FREQ RESP H1      MAG                    MAIN  Y:  -147.5dB
Y:    50.0dB      80dB                        X:   3200Hz
X:    0Hz + 3.2kHz      LIN
SETUP W2      #A: 30
```

```
8    IMPULSE RESP      MAG                    REF    Y:   53.5dB
Y:    80.0dB      40dB                        X:   ▓▓▓▓▓
X:    0.00ms + 125ms                          ΔX:  48.95ms
SETUP W2      #A: 30                b)         ΔY     : -8.7dB        840116
```
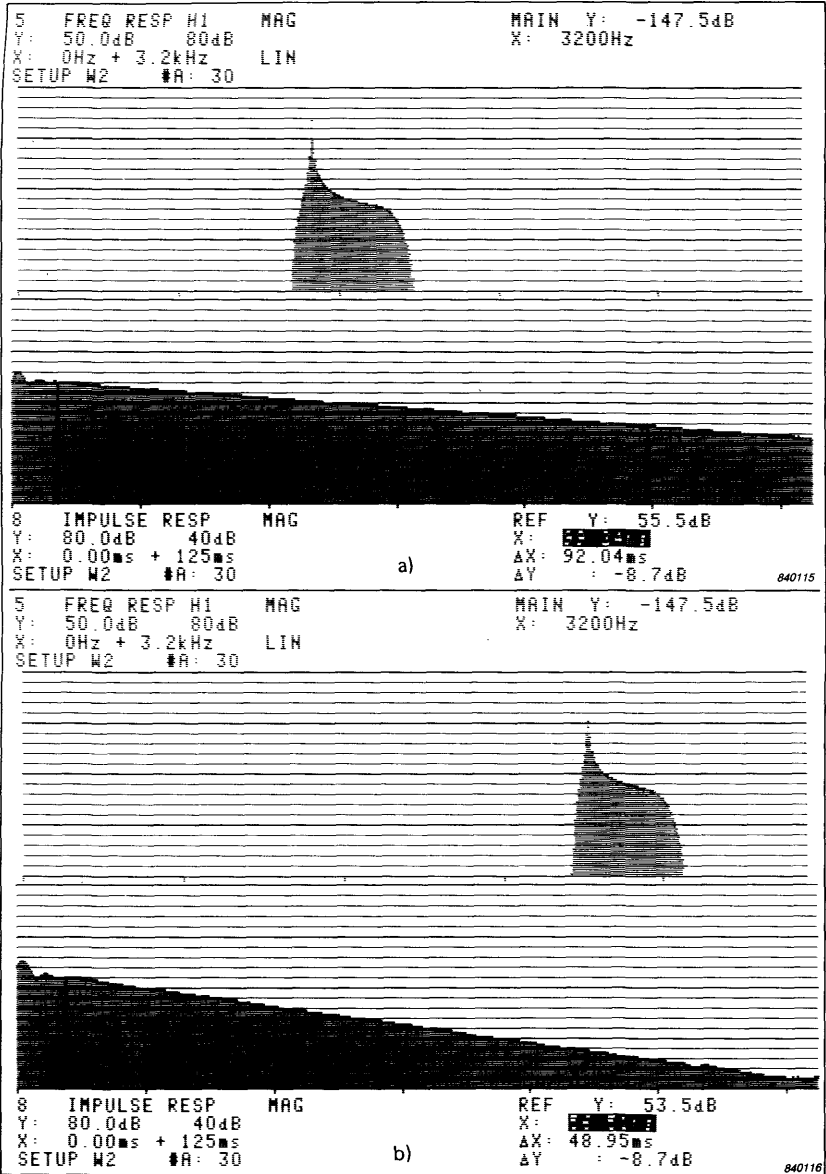
Fig. 41. a)   Extraction of the second resonance and the corresponding Impulse Response Function

b)   Extraction of the fifth resonance with the corresponding Impulse Response Function.

A zoom analysis, using random noise excitation and a resolution of 0,25 Hz (compared to a resolution of 4 Hz in the baseband measurement) on each of the three resonances (first, second and fifth resonance) gave the following 3dB bandwidths:

Δf_1 = 3,10 Hz, Δf_2 = 3,15 Hz and Δf_5 = 6,25 Hz

The corresponding decay rates are:
σ_1 = 9,8 rad/s, σ_2 = 9,9rad/s and σ_5 = 19,7rad/s,

corresponding quite well with the results from the Impulse Response Functions. Since each zoom analysis is 16 times slower than the baseband analysis (16 times higher resolution) the total analysis time for the three resonances is 3 x 16 = 48 times longer when using zoom analysis compared to the baseband and Impulse Response Function method.


```
5    FREQ RESP H1    MAG                MAIN  Y:  29.1dB
Y:   50.0dB    80dB                     X:   ▓▓▓▓▓
X:   0Hz + 3.2kHz   LIN
SETUP W1    #A: 4                       [ ]
```

```
8    IMPULSE RESP    MAG                REF   Y:  51.0dB
Y:   80.0dB    40dB                     X:   62.98ms
X:   0.00ms + 125ms                     ΔX:  52.12ms
SETUP W1    #A: 4                       ΔY   : -8.7dB
                                                   840117
```
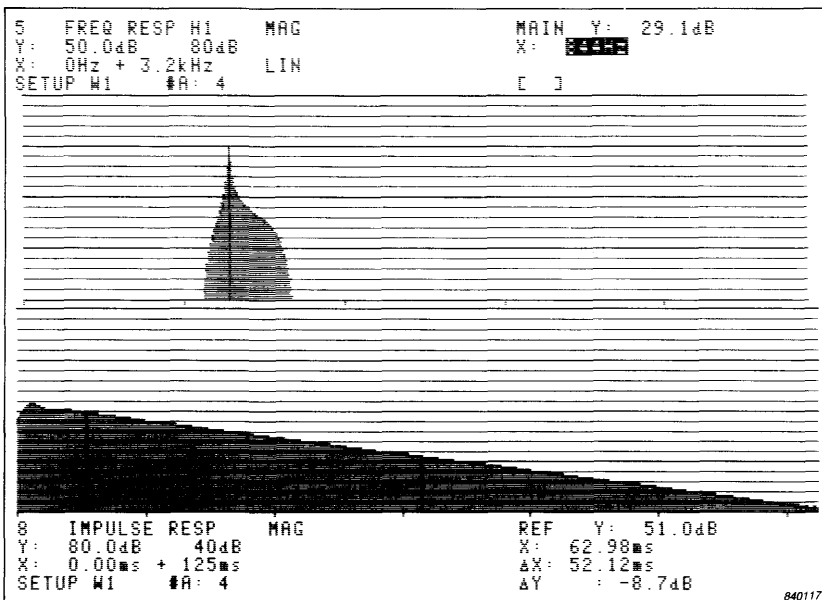
Fig. 42. Same Frequency Response Function as in Fig.38, here measured by use of Impact Hammer excitation. The first resonance is extracted by use of a weighting function (upper graph) and the corresponding Impulse Response Function (magnitude of) is shown with logarithmic amplitude scale in the lower graph

17

Impact hammer excitation can also be used for the test, and the baseband analysis and Impulse Response Function method can be applied. The extra artificial damping caused by the exponential weighting function, which might be applied on the response signal in Channel B, is known and can be corrected for as explained in Section 5.6. Fig.42 shows the edited driving point accelerance for the same structure, point and direction as used before (Fig.38). The analysis bandwidth of 4 Hz is also the same. The first resonance is extracted by use of the same weighting function as used in the lower graph of Fig.38 and shown in Fig.39. The time constant of the Impulse Response Function is found to be τ_1 = 52,12ms. The exponential weighting which was applied on the response signal had a length (time constant) of τw = 99,97ms. Thus the true decay rate is

$$\sigma_1 = \frac{1}{\tau_1} - \frac{1}{\tau_w} = 19,18\text{rad/s} - 10,00\text{rad/s} = 9,18\text{rad/s},$$

which is the same, within 5% accuracy, as the decay rate found in the test using pseudo-random excitation with a shaker.

7. Autocorrelation and Cross Correlation

The mathematical definitions of the Autocorrelation Function $R_{aa}(\tau)$ of a signal $a(t)$ and the Cross Correlation Function $R_{ab}(\tau)$ between two signals $a(t)$ and $b(t)$ are given by

$$R_{aa}(\tau) = \lim_{T \to \infty} \frac{1}{T} \int_T a(t)\, a(t+\tau)\, dt \qquad (7.1)$$

$$R_{ab}(\tau) = \lim_{T \to \infty} \frac{1}{T} \int_T a(t)\, b(t+\tau)\, dt \qquad (7.2)$$

Comparing these definitions to the definition of covariance σ_{ab} between two variables a and b given by (3.2) it is seen, apart from the subtraction of the mean values μ_a and μ_b in σ_{ab}, that the Autocorrelation $R_{aa}(\tau)$ is the covariance of the time signal $a(t)$ and a replica of this signal displaced τ in time i.e. $a(t+\tau))$. Likewise, the Cross Correlation $R_{ab}(\tau)$ is the covariance of $a(t)$ and the time signal $b(t)$ with a displacement of τ in time i.e. b(t+τ).

The practical interpretation of Autocorrelation Function $R_{aa}(\tau)$ is therefore to what degree the time signal $a(t)$ is similar with a displaced version of itself as a function of the displacement τ. Likewise the Cross Correlation Function $R_{ab}(\tau)$ gives a measure of the degree of similarity

between the time signal *a(t)* and a displaced version of the time signal *b(t) as* a function of the time displacement т.

In practice it is often more convenient to work with the normalised Correlation Functions given by:

$$\rho_{aa}(\tau) = \frac{R_{aa}(\tau)}{R_{aa}(0)} \qquad (7.3)$$

and

$$\rho_{ab}(\tau) = \frac{R_{ab}(\tau)}{\sqrt{R_{aa}(0)\ R_{bb}(0)}} \qquad (7.4)$$

$\rho_{aa}(\tau)$ and $\rho_{ab}(\tau)$ are called the Autocorrelation Coefficient Function and the Cross Correlation Coefficient Function respectively. $R_{aa}(0)$ is the total power in the signal a(t) given by

$$\lim_{T \to \infty} \frac{1}{T} \int_T a^2(t)\, dt$$

and $R_{bb}(0)$ is the total power in the signal *b(t)* given by

$$\lim_{T \to \infty} \frac{1}{T} \int_T b^2(t)\, dt.$$

It can be shown that $| \rho_{aa}(\tau) | \leq 1$ and that $| \rho_{ab}(\tau) | \leq 1$ for all т.

$\rho_{aa}(\tau)$ and $\rho_{ab}(\tau)$ correspond to the Correlation Coefficient ρ_{xy} defined by (3.1).

From (7.1) and (7.2) it is easily shown (using the convolution theorem for the Fourier Transform) that the Autocorrelation Function $R_{aa}(\tau)$ and the Cross Correlation Function $R_{ab}(\tau)$ are related to the Autospectrum $S_{AA}(f)$ and the Cross Spectrum $S_{AB}(f)$ via the Fourier Transform as:

$$R_{aa}(\tau) = \mathcal{F}^{-1} \left\{ S_{AA}(f) \right\} = \int_{-\infty}^{\infty} S_{AA}(f)\, e^{j2\pi f\tau}\, df \qquad (7.5)$$

and

$$R_{ab}(\tau) = \mathcal{F}^{-1} \left\{ S_{AB}(f) \right\} = \int_{-\infty}^{\infty} S_{AB}(f)\, e^{2\pi f\tau}\, df \qquad (7.6)$$

When $R_{aa}(\tau)$ and $R_{ab}(\tau)$ are calculated from a dual channel FFT measurement, (7.5) and (7.6) are used as seen in Fig.2 (Section 2). The inverse Fourier Transform performed in practice is of course the inverse DFT (or rather inverse FFT) as discussed in Section 2.1.

Since $S_{AA}(f)$ is real and even $R_{aa}(\tau)$ is also real and even i.e. $R_{aa}(\tau) = R_{aa}(-\tau)$. $R_{ab}(\tau)$ is also real, because $S_{AB}(f)$ is conjugate even, but is in general **not** even, because $S_{AB}(f)$ in general have an imaginary part different from zero.

The obvious applications of the **Autocorrelation Function** are:

a) Detection of echoes (reflections) in the signal.
If an echo (reflection) with a time delay of τ_o exists in the signal, the Autocorrelation Function will peak at $\tau = \tau_o$ (apart from at $\tau = 0$) and the value of the Autocorrelation Coefficient Function at τ_o, $\rho_{aa}(\tau_o)$,' will give a measure of the relative strength of the echo (reflection). It is here assumed that the signal is a broadband signal, which will become clear shortly.

b) Detection of periodic signals buried in random noise
The Autocorrelation Function of a periodic signal is also periodic, since a periodic signal will correlate with itself at a delay of one period T, two periods $2\,T$, etc. The random background noise signal will have an Autocorrelation Function which diminishes to zero with increasing delay and the periodic signal can therefore be detected after a certain delay time in the Autocorrelation Function.

Fig.43 shows the Autocorrelation Coefficient Function ρ_{aa} for a) broadband random noise, b) sinewave and c) sinewave buried in broadband random noise.

The Autocorrelation Coefficient Function for the broadband random noise diminishes very quickly to zero (Fig.43.a)). This is a consequence of the socalled uncertainty principle for functions related by the Fourier Transform. If the bandwidth of the Autospectrum $G_{AA}(f)$ is Δf and the width of the Autocorrelation Function $R_{aa}(\tau)$ is Δt, the uncertainty principle states that

$$\Delta f \cdot \Delta t \geq 1 \qquad\qquad (7.7)$$

In the example, Fig.43 a), the bandwidth of the random noise is $\Delta f \approx$ 1040 Hz and it is seen that $\rho_{xy}(\tau) \approx 0$ for $\tau = \Delta\,t = 1,4$ ms $\geq \dfrac{1}{\Delta f} = 0,96$ms.

The Autocorrelation Coefficient Function for the sinewave is a cosine with the same period length T as shown in Fig.43.b). The sinewave correlates 100% with itself with delays of $\tau = 0$, $\tau = 1$ period length, $\tau = 2$ period lengths etc. In Fig.43.b) the period length is 1,251 ms (see cursor readout ΔX).
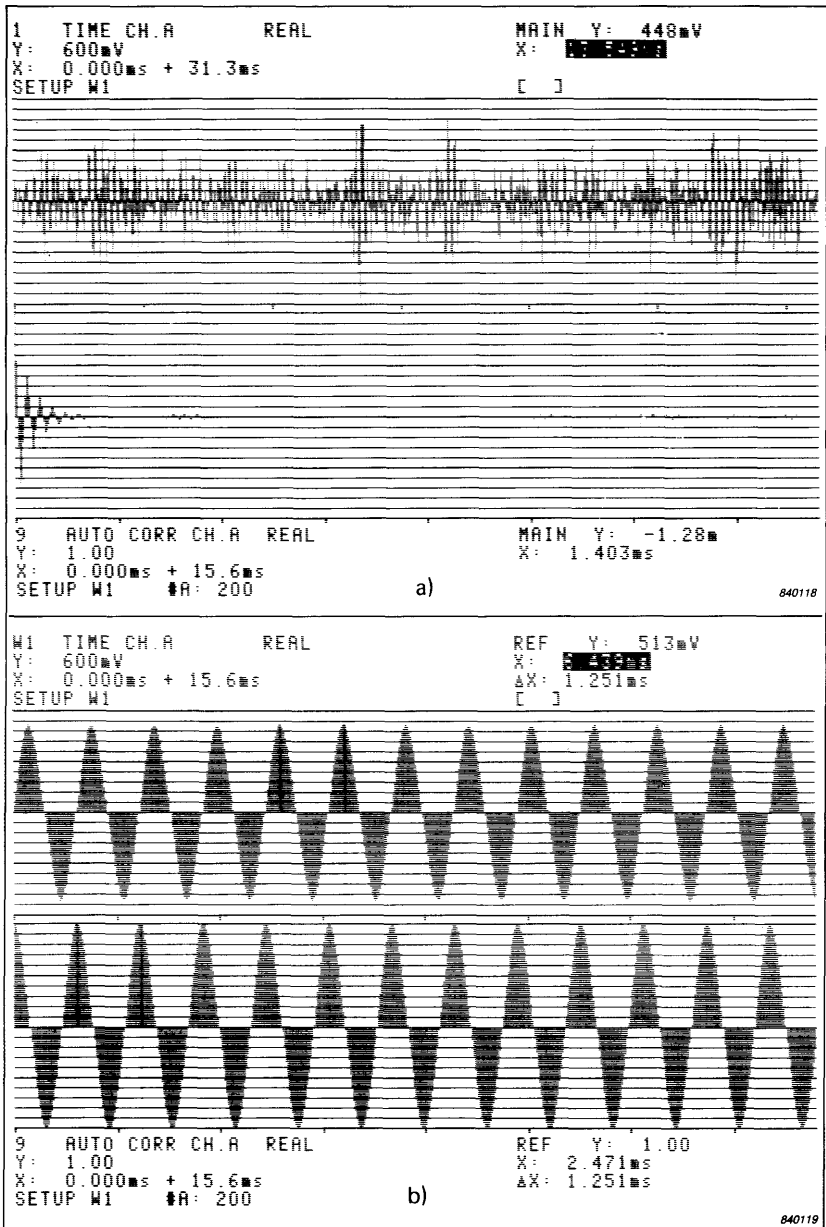
Fig. 43. Autocorrelation Coefficient Function for different types of signals
a) Broadband random noise b) Sine wave

```
W1   TIME CH.A      REAL            MAIN  Y:   65.9mV
Y:   100mV                          X:    ███████
X:   0.000ms + 15.6ms
SETUP W1                            [   ]
```

```
9    AUTO CORR CH.A  REAL           REF   Y:   150m
Y:   1.00                           X:    2.914ms
X:   0.000ms + 7.81ms               ΔX:   0.411ms
SETUP W1    #A: 200          c)
```
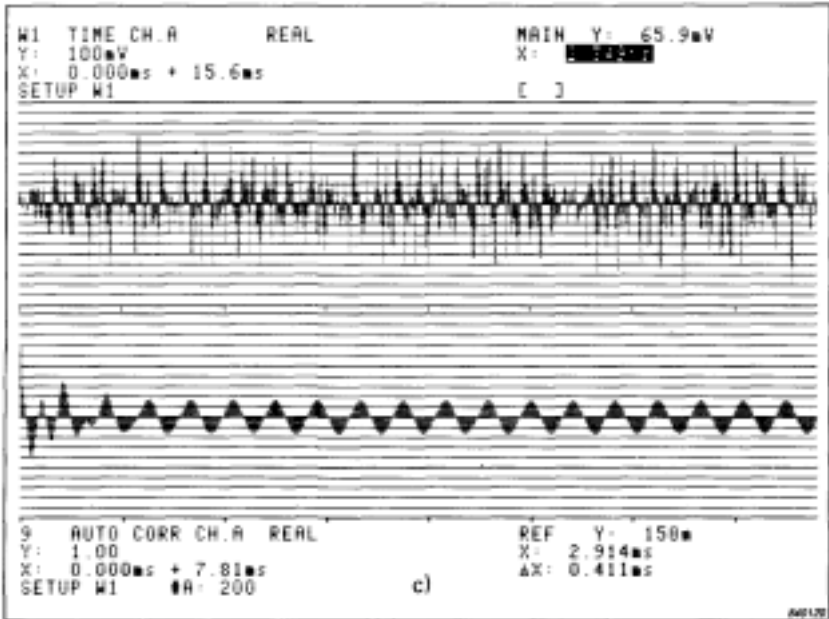
Fig. 43. Autocorrelation Coefficient Function for different types of signals
c) Sine wave buried in broadband random noise

It is thus obvious that detection of echoes (reflections) can only be performed using the Autocorrelation Function if the signal is broadband and with enough bandwidth that the corresponding peaks in the Auto-correlation Function become sufficiently narrow and well separated.

It should be mentioned that for this application, use of the Cepstrum is often preferred over use of the Autocorrelation Function, since the Cepstrum is less sensitive to the shape of the Autospectrum. A description of Cepstrum techniques is found in Ref. [14].

In Fig.43.c) it is seen that the Autocorrelation Coefficient Function detects the periodic signal (a sinewave) which is buried in the random background noise.

If the periodic signal is a signal containing several frequency compo-nents it might be more suitable to use the Autospectrum rather than the Autocorrelation Function since the frequencies of the different compo-

22

nents and their levels are directly detected in the Autospectrum. Zoom analysis might however be required if their levels are very low compared to the background noise level.

The most common applications of **Cross Correlation Function** are the following:

a) **Determination of time delays.** If a signal is propagating from one point A to another point B the Cross Correlation Function $R_{ab}(\tau)$ between the signals $a(t)$ and $b(t)$ at the two points will have a peak at the time displacement corresponding to the time delay (propagation time) τ between the two points. It is assumed that the signals involved are broadband and that the propagation is non-dispersive which means that propagation velocity is independent of frequency. If the velocity depends upon the frequency the propagation is said to be dispersive and this will complicate the situation. There are two possibilities of getting around this problem.

One possibility is to apply a weighting function on the Cross Spectrum (similar to the weighting functions applied on the Frequency Response Function described in Section 6), before the inverse Fourier Transform, in order to find the Cross Correlation Function for only a limited frequency range, where the propagation velocity can be considered as nearly constant. The peak in the Cross Correlation Function will of course be smeared out as a consequence of the uncertainty principle (7.7).

Another possibility is to use the phase of the Cross Spectrum directly, since this is related to the delay time. For a single delay of $\tau_o(f)$ the phase of the Cross Spectrum is $\Phi_{AB}(f) = 2\pi f \tau_o(f)$ and the time delay can thus be found as a function of frequency $\tau_o(f)$.

b) **Identification of transmission paths.** If there are several transmission paths for the signal from point A to point B there will be several peaks in the Cross Correlation Function, one peak for each transmission path at a delay time τ_n corresponding to the propagation time τ_n for the nth path. The amplitude of each peak in the Cross Correlation Coefficient Function will give a measure of the relative strength of each transmission path. Again it is here assumed that the signals are broadband and that the propagation is non-dispersive. If the propagation is dispersive, application of weighting functions on

the Cross Spectrum before the inverse Fourier Transform as described under a) might still make identification of transmission paths possible.

c) **Detection of signals buried in extraneous noise.** If a signal $s(t)$, which can be either deterministic or random, is buried in extraneous noise in both $a(t)$ and $b(t)$ i.e. $a(t) = s(t) + n(t)$ and $b(t) = s(t) + m(t)$, where $n(t)$ and $m(t)$ *are* assumed to be uncorrelated, the Cross Correlation Function $R_{ab}(\tau)$ will only contain information about the correlated part $s(t)$ in $a(t)$ and $b(t)$.

This is because the uncorrelated noise terms $n(t)$ and $m(t)$ at each frequency will be averaged out in the Cross Spectrum $S_{AB}(f)$ which therefore will only contain contribution from the correlated parts in $a(t)$ and $b(t)$ *as* explained in Section 2.1. In the situation considered here the Cross Correlation Function $R_{ab}(\tau)$ will give the Autocorrelation Function $R_{SS}(\tau)$ of the signal $s(t)$ without any influence from $n(t)$ and $m(t)$.

Fig.44 illustrates the applications a) and b). In this acoustical experiment the input is measured with a microphone close to a sound source and the output is measured with a microphone at a distance of approximately 1,1m.

The source generates broadband random noise and the input Autospectrum $G_{AA}(f)$ (upper graph of Fig.44) is seen to be fairly flat over the frequency range considered (0-12,8 kHz). The Cross Correlation Coefficient Function $\rho_{ab}(\tau)$. shown in the middle graph, reveals a number of propagation paths (direct sound and reflections). The peaks corresponding to the different paths are narrow, because the signals are broadband and it is quite easy to separate the paths and find their propagation times.

Fig.45 shows similar results when the source is fed by band-limited random noise. The Cross Correlation Coefficient Function $\rho_{ab}(\tau)$ (the graph in the middle) again reveals the different propagation paths, but the peaks are now very broad due to the frequency band limitation of the signals involved. The broadening of the peaks complicates the identification of the different reflections which illustrates one of the difficulties often encountered in practice.
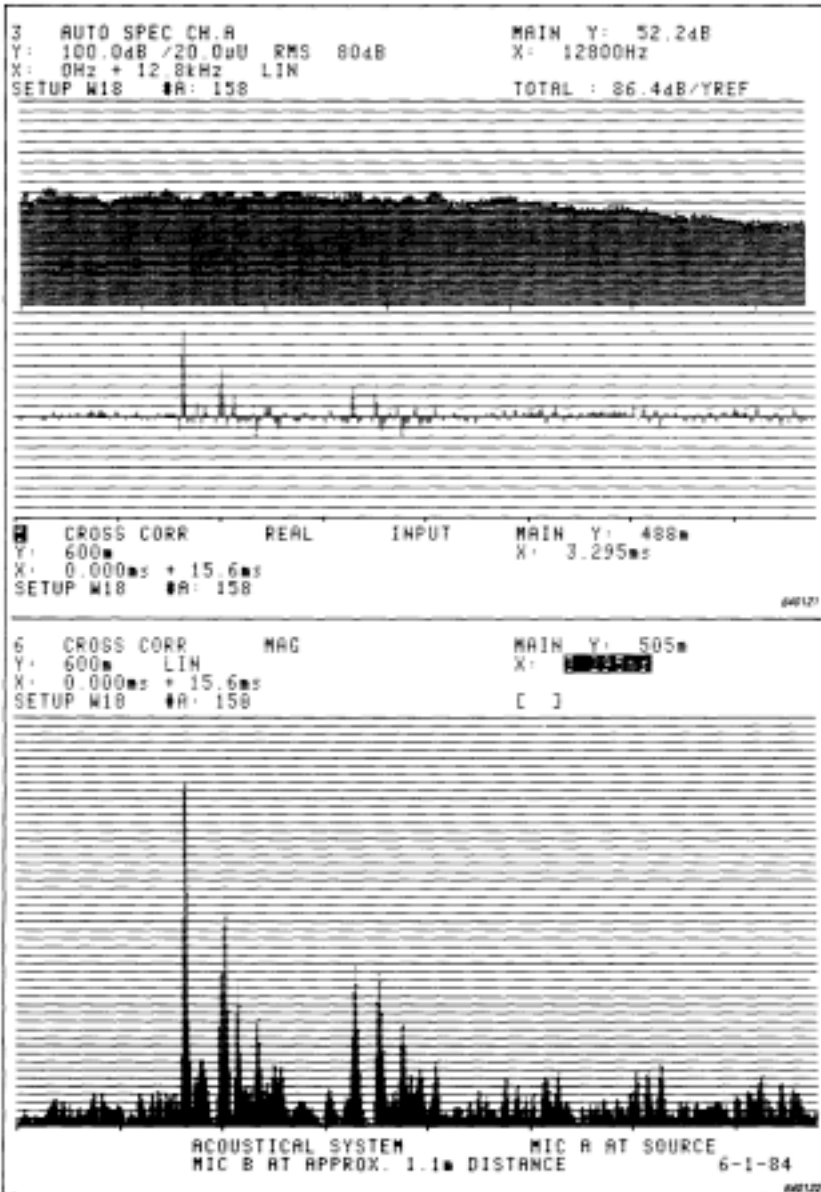
24

```
3    AUTO SPEC CH.A                    MAIN  Y:  52.2dB
Y:   100.0dB /20.0uU   RMS   80dB     X:   12800Hz
X:   0Hz + 12.8kHz     LIN
SETUP W18    #A: 158                  TOTAL : 86.4dB/YREF
```

```
#    CROSS CORR      REAL       INPUT    MAIN  Y:  488m
Y:   600m                                X:   3.295ms
X:   0.000ms + 15.6ms
SETUP W18    #A: 158
```

```
6    CROSS CORR      MAG                 MAIN  Y:  505m
Y:   600m    LIN                         X:   [      ]
X:   0.000ms + 15.6ms
SETUP W18    #A: 158                     [  ]
```

```
ACOUSTICAL SYSTEM            MIC A AT SOURCE
MIC B AT APPROX. 1.1m DISTANCE            6-1-84
```
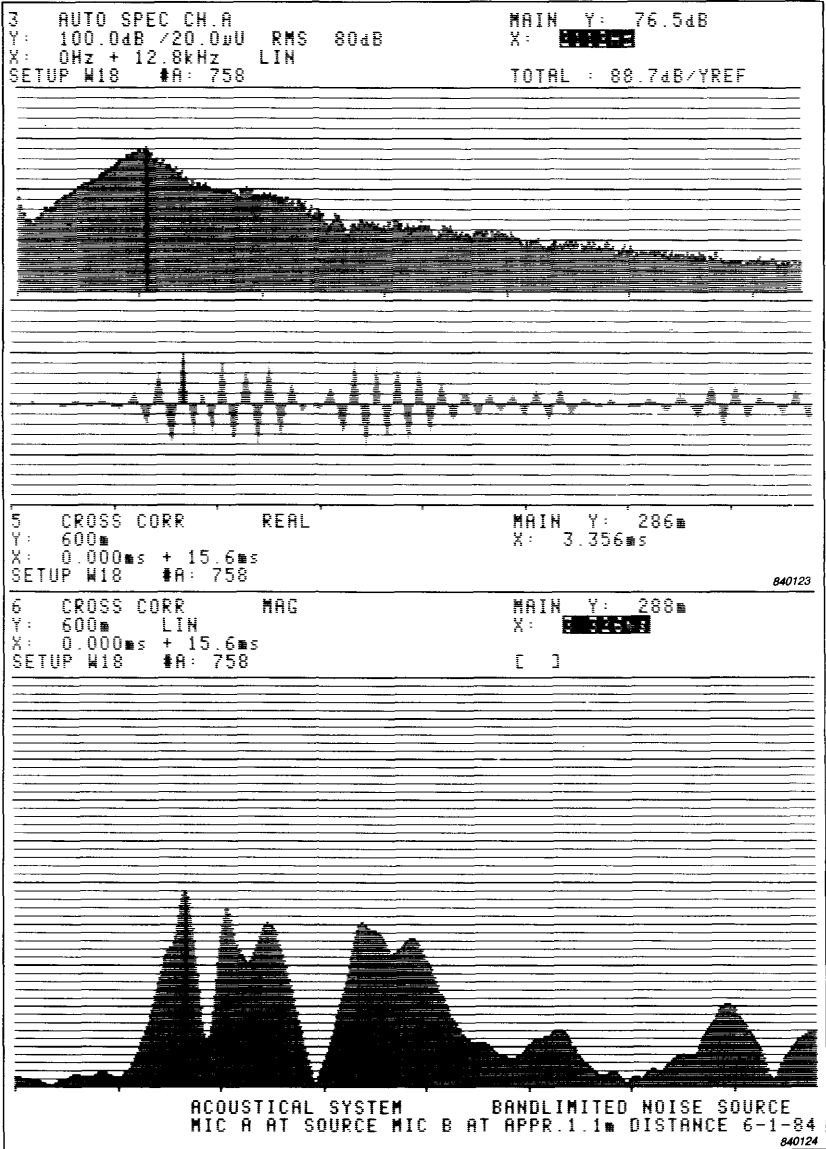
Fig. 44. The input Autospectrum of a broadband random noise signal from a sound source (upper graph). Real valued $\rho_{ab}(\tau)$ (middle graph). Magnitude of the complex $\check{\rho}_{ab}(\tau)$ (lower graph)

```
3     AUTO SPEC CH.A                      MAIN  Y:  76.5dB
Y:    100.0dB /20.0µU  RMS   80dB         X:   ▪▪▪▪▪▪
X:    0Hz + 12.8kHz    LIN
SETUP W18   #A: 758                       TOTAL :  88.7dB/YREF
```

```
5     CROSS CORR      REAL                MAIN  Y:  286m
Y:    600m                                X:   3.356ms
X:    0.000ms + 15.6ms
SETUP W18   #A: 758                                        840123
```

```
6     CROSS CORR      MAG                 MAIN  Y:  288m
Y:    600m    LIN                         X:   ▪▪▪▪▪▪
X:    0.000ms + 15.6ms
SETUP W18   #A: 758                       [   ]
```

```
              ACOUSTICAL SYSTEM          BANDLIMITED NOISE SOURCE
              MIC A AT SOURCE MIC B AT APPR.1.1m DISTANCE 6-1-84
                                                              840124
```

Fig. 45. The input Autospectrum of a band limited random noise signal from the sound source (upper graph). Real valued $\rho_{ab}(\tau)$ (middle graph). Magnitude of the complex $\check{\rho}_{ab}(\tau')$ (lower graph)

In other words, the signals have to be so broadband that the peaks in the Cross Correlation Function become narrow and separated, exactly as discussed for application of Autocorrelation Function for detection of echoes.

For the same reasons, as those mentioned for the analytical Impulse Response Function $\overset{\triangledown}{h}(t)$ in Section 6, it is an advantage in many situations to work with the analytical Autocorrelation Coefficient Function $\overset{\triangledown}{\rho}_{aa}(\tau)$ and the analytical Cross Correlation Coefficient Function $\overset{\triangledown}{\rho}_{ab}(\tau)$ rather than with the real valued $\rho_{aa}(\tau)$ and $\rho_{ab}(\tau)$- These are defined by:

$$\overset{\triangledown}{\rho}_{aa}(\tau) \ = \rho_{aa}(\tau) + j\rho_{aa}(\tau) \tag{7.8}$$

and

$$\overset{\triangledown}{\rho}_{ab}(\tau) \ = \rho_{ab}(\tau) + j\rho_{ab}(\tau) \tag{7.9}$$

where $-\rho_{aa}(\tau)$ and $-\rho_{ab}(\tau)$ are the Hilbert Transforms of $\rho_{aa}(\tau)$ and $\rho_{ab}(\tau)$ respectively. The lower graphs in Fig.44 and 45 show the magnitude of the analytical Cross Correlation Coefficient Functions corresponding to the real valued Cross Correlation Coefficient Functions
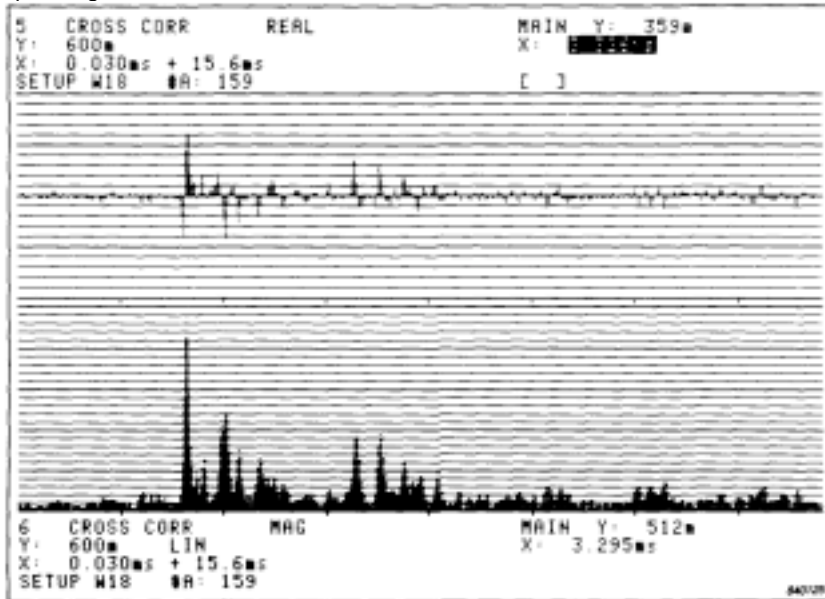
Fig. 46. Same results as for Fig.44, but obtained with zoom analysis between 512 and 13312 Hz

shown in the graphs in the middle. The peaks are easier to identify since the oscillations in $\rho_{ab}(\tau)$ are avoided. This is specially an advantage in the situation with band limitation as in Fig.45. If a zoom analysis is performed, the magnitude $|\overset{\triangledown}{\rho}_{ab}(\tau)|$ should also be used for measurement of the peak amplitudes for the different reflections, since the real part $\rho_{ab}(\tau)$ might not peak where $|\overset{\triangledown}{\rho}_{ab}(\tau)|$ peaks. Fig.46 illustrated this where the exact same signals as in Fig.44 are analysed, however using a zoom analysis from 512Hz to 13312hz. This frequency range covers all the important information as does the baseband frequency range used in Fig.44. In the real part $\rho_{ab}(\tau)$, an amplitude for the peak at 3,3ms is found to be 0,36, while the magnitude $|\overset{\triangledown}{\rho}_{ab}(\tau)|$ gives an amplitude of 0,51 which is the same as the amplitude found in Fig.44.

In Fig.47 the magnitude of the Cross Spectrum $G_{AB}(f)$ and the magnitude of the Cross Correlation Coefficient Function are shown for the same signals, as those analyzed by use of the Impulse Response Function in Fig.37 (Section 6). The main reflections can still be seen in the Cross Correlation Coefficient Function, but their peaks are so
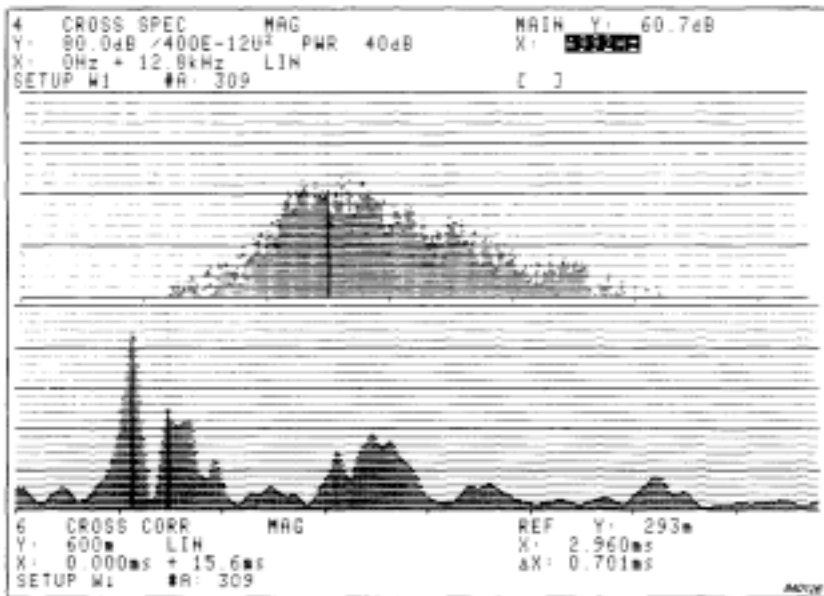
Fig. 47. *Magnitude of Cross Spectrum and*
Magnitude of Cross Correlation Coefficient Function of the same signals as those analyzed by Impulse Response Function in Fig.37.

smeared out, due to the band limitation seen in the Cross Spectrum, that some of the smaller reflections are not detected. Fig.37 shows that the Impulse Response Function is insensitive to this band limitation of the input signal, since it describes the system independent of the signals involved.

Note that there has to be some power in the input signal at all the frequencies in the analysis bandwidth, before a well-defined Frequency Response Function (and thereby a well-defined Impulse Response Function) can be computed.

Since we are working with the DFT (or rather FFT) which computes the spectra at discrete frequencies, the effect of circular correlation has to be taken into account. As a consequence of computing the spectra at discrete frequencies $k \Delta f = k^1/T$, the time signals are artificial period signals ranging from $-\infty$ to $+\infty$ with the time record in the analyzer of length T being the period length. The computed Correlation Functions are the Correlation Functions of these artificial periodic time signals displaced relative to each other, and a circular correlation effect, as shown in Fig.48, will appear. The end of one signal (end of the period in one signal) will overlap with the beginning of the other signal (the beginning of the period in the other signal) and the estimated Correlation Function will be incorrect. In Fig.48 (lower graph) the Correlation Func-
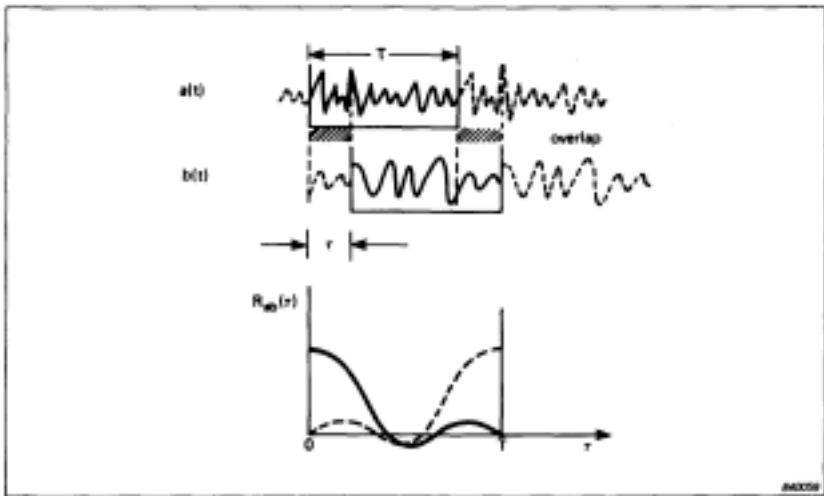

Fig. 48. Circular correlation effect. The Correlation Function is assumed to be even in the lower graph
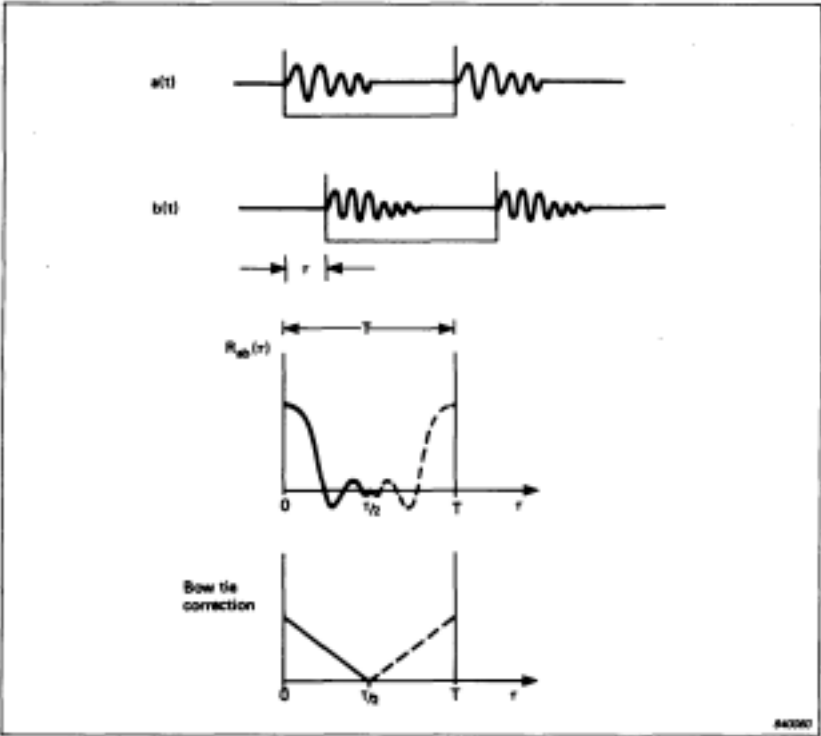
Fig. 49. Zero pad of the time records in order to avoid the effect of the
circular correlation shown in Fig.48. The bow tie correlation is
shown in the lower graph

tion between the two signals is assumed to be even, which is not the
case in general for Cross Corrleation Functions. This problem of circular
correlation is overcome by setting the signal equal to zero in the second
half of the record as illustrated in Fig.49. This is called "zero pad". The
zero pad will, however, also cause the estimated Correlation Function to
be biased, but the bias error is known and can be corrected for. Due to
the artificial nullifying of the signals in the last half of the record the
estimated Correlation Function $\hat{R}(\tau)$ will be lower than the true Correla-
tion Function $R(\tau)$, the extent depends upon the displacement τ. The
relation is

$$\hat{R}(\tau) = \frac{|T/2 - \tau|}{T/2} \ R(\tau) \ ; \ 0 \le \tau \le T/2 \tag{7.10}$$

assuming rectangular weighting in the analysis.

30

Correction for the factor $\dfrac{|^{T}\!/_2 - \tau|}{^{T}\!/_2}$ is called the "bow tie" correction (see Fig.49) and can be applied as a post-processing after the measurement.

In Fig.49 the Correlation Function $R(\tau)$ is assumed to be even (as in Fig.48), which only in general is true for Autocorrelation Functions.

In all the measurements shown in this Section, zero pad and rectangular weighting has been used.

If the signals involved are transients with a duration shorter than $^{T}\!/_2$, the bow tie correction should obviously not be used.

8. Sound Intensity

The sound intensity is a vector quantity $\vec{I}$ describing the direction and the amount of the net flow of acoustic energy at a given position in a sound field.

A dual channel FFT measurement of the sound pressure signals from two closely spaced microphones can be used for calculation of the sound intensity. The calculated intensity is the component I_r of the intensity vector $\vec{I}$ in the direction given by the line joining the acoustic centres of the two microphones.

Fig.50 shows a microphone probe where the two microphones are placed in a face to face configuration (the B&K Sound Intensity Probe Type 3519). This sound intensity probe features very little disturbance of the sound field. The shadowing effect of one microphone on the other is minimal and the effective separation between the microphones is well
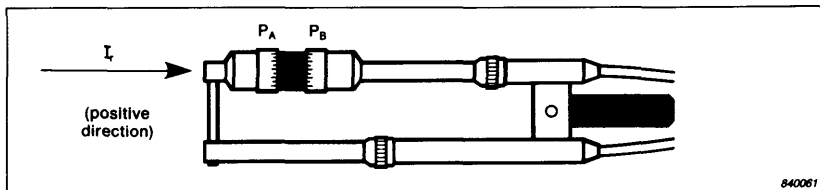

Fig. 50. Two microphone sound intensity probe (B&K Type 3519) with the microphones in face to face configuration. The component I_r of the sound intensity vector $\vec{I}$, is measured positive in the direction indicated by the arrow (from microphone A to microphone B)

31

defined. A side by side configuration of the microphone is also used sometimes, for instance in situations where the space is very confined or when measurements has to be performed as close as possible to a surface.

It can be shown that the intensity component I_r, with the direction from microphone *A* to microphone *B* defined as the positive direction, is given by

$$I_r = -\frac{1}{\omega\rho\Delta r}\ Im\ \{G_{AB}(f)\} \tag{8-1}$$

where $Im\ \{G_{AB}(f)\}$ is the imaginary part of the one-sided Cross Spectrum between the two sound pressure signals $p_A(t)$ and $p_B(t)$, ρ is the density of air and Δr is the spacing between the microphones. The air density is given by the ambient pressure p (in mbar) and the air temperature t (in °C) via the formula

$$\rho = 0{,}3485\ \frac{p}{273+t}\ [\frac{kg}{m^3}]$$

In the B&K Analyzers Types 2032 and 2034, the microphone spacing Δr, the ambient pressure p and temperature t are entered from the front panel and the sound intensity is calculated according to (8.1) from the basic dual channel measurement. The sound pressure Autospectra $G_{AA}(f)$ and $G_{BB}(f)$ are therefore available as well from the same measurement. The reactivity of the sound field defined as $L_K = L_I - L_P$, where L_I is the intensity level (in dB relative to 1 pW/m^2) and L_P is the sound pressure level (in dB relative to 20 μ Pa), can be checked from the same measurement. The reactivity L_K should always be checked, since it is one of the factors which determines the statistical errors in the intensity estimates and should be within the dynamic range of the analysis. For a plane wave propagating in free field the reactivity is zero dB ($L_P = L_I$) and the sound field is called an active sound field. In an ideal diffuse field the intensity is zero and the sound field is purely reactive.

The sound intensity can also be calculated directly in real time using the formula

$$I_r = -\frac{1}{2\ \rho\ \Delta r}\ \overline{(p_A + p_B)\int (p_B - p_A)\ dt} \tag{8.2}$$

where the bar indicates time averaging and p_A and p_B are the sound pressure time signals as before. This approach is implemented using $^1/_3$ octave and $^1/_1$ octave (and $^1/_{12}$ octave) digital filters in the B&K Intensity Analyzer Type 3360.

Compared to this technique one of the advantages of using the two channel FFT approach to sound intensity is that, since the spectrum is calculated in narrow bands with constant bandwidth, this method is very suitable for detection and recognition of pure tones, in a sound field. There might be several closely spaced pure tones, coming from different directions, which can only be separated using narrow band analysis, assuming that these frequency components are sufficiently stable. Harmonic related frequency components in the sound field can also easily be identified using constant narrow bandwidth and a linear frequency scale. Fig.51 shows an example where the B&K Analyzer Type 2032 is used. The sound intensity is shown on a socalled bipolar display, where positive intensity components point upwards in the upper half of the display and negative intensity components point downwards in the lower half of the display. One sound source is seen to radiate harmonic related frequency components in a direction towards the front of the probe and gives a resulting positive intensity level at these frequencies. Another source, which radiates broadband random noise in the opposite direction at the probe position, is causing the net flow of acoustical energy, in the direction of the probe, to be negative at the other frequencies.

One of the disadvantages of using the two channel FFT approach as opposed to the digital filter method is that the analysis can only be performed in real time in a limited frequency span. Since Hanning weighting is used when analyzing normal continuous signals, there has
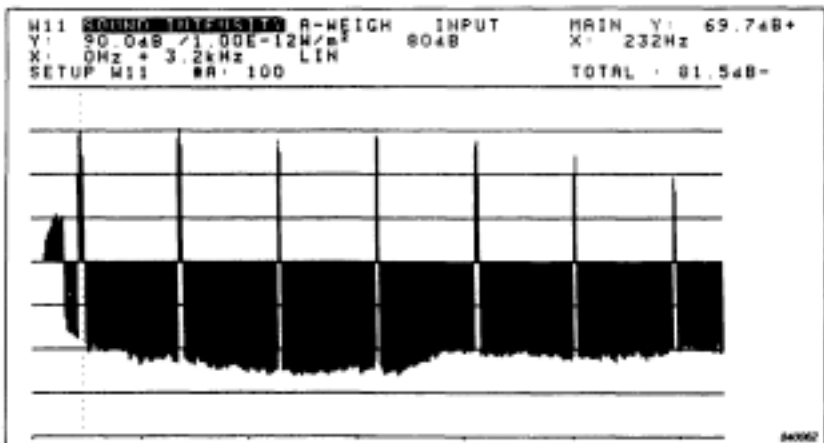

Fig. 51. Example of a narrow band sound intensity spectrum, calculated from a two channel measurement (B&K Analyzer Type 2032 or 2034)

to be 75% overlap of the time records in order to get true real time analysis, i.e. a resulting (overall) weighting function on the time signals which is flat (see Ref.16). This means for instance that for the high speed B & K Analyzer Type 2032 a true real time analysis can only be performed in a frequency span which is not wider than $\sim^1/_4$ x 5 kHz. The digital filter Analyzer Type 3360 will always work in real time up to 10kHz in the $^1/_3$ octave and $^1/_1$ octave mode.

Another disadvantage of the two channel FFT approach is that longer averaging time is needed in order to get the same statistical accuracy in the measurement as by use of the digital filter analyzer, except for very low frequencies. The broader bandwidths of the $^1/_3$ octave or $^1/_1$ octave filters give an averaging in frequency which will decrease the random error (see Section 9). Specially if the sound field is very reactive (high sound pressure level compared to the intensity level) as in diffuse sound fields, the sound intensity measurement using two channel FFT can be very time consuming in order to obtain a certain statistical accuracy of the estimated sound intensity spectrum.

Consider an example where a number of averages n_d = 500 is required in order to get a specified statistical accuracy.

a) FFT Method:
   Let us assume that we are working with a frequency span which is so wide that the analysis time for computing one sound intensity spec-trum, is longer than the record length in the analyzer. For the high speed B&K Analyzer Type 2032, this means that the frequency span is wider than 5kHz. One sound intensity spectrum is computed approximately every 160msec giving a total analysis time of $T_{total} \approx$ 500 x 160 msec = **1 min 20 sec.**

b) Digital Filter Method:
   n_d = *500* is equivalent to a BT product (Bandwidth x Averaging Time) of 500. For the $^1/_3$ octave at 1 kHz, for instance, B $\approx$ 230 Hz and the

   total analysis time is therefore $T_{Total} = \dfrac{500}{B} \approx$ **2,2 sec.** For the $^1/_3$ oc-tave filter at 10kHz, $T_{Total} \approx$ **0,22sec** and for the $^1/_3$ octave filter at 100 Hz, $T_{Total} \approx$ **22 sec.**

For many applications it is also much easier to handle and interpret the reduced amount of data from a $^1/_3$ octave or a $^1/_1$ octave analysis. Since acoustic measurements are often specified in $^1/_3$ octave or $^1/_1$ octaves, an analysis using the system with the standardized filters would be preferred.

Finally it should be mentioned that the digital filter system Type 3360 is a dedicated intensity measurement system giving some practical advantages for the user, such as a remote control unit and a separate display unit.

The basic limitations in the two microphone approach to analysis of sound intensity are the same for both systems. The finite distance Ar between the two microphones gives an upper bound for the useful frequency range in the analysis, and the phase mismatch between the two channels in the measurement system, including the microphones, gives a lower limit on the frequency range. A discussion of this is found in Ref.15 and 22.

The principal applications of sound intensity are: a) sound power determination, b) ranking of noise sources, c) noise source location (for this purpose it is often useful to make an intensity mapping in terms of contour plots or 3-D plots, made by use of further post-processing and plotting routines), d) transmission loss determination, e) sound absorption measurements.

Examples of these applications are dealt with in the References [15, 20, 21, 27-30] and will not be discussed further in this article.

9. Statistical errors in the estimates

When the analysis is performed on random signals (time histories) the different functions derived from a dual channel FFT measurement are estimated with limited accuracy. It is here assumed that we have stationary, continuous or transient random signals, which are band-limited Qaussian distributed white noise signals over the analysis bandwidth.

Averaging of the Autospectra and the Cross Spectrum is performed over only a finite number of records n_d giving the estimates $\hat{S}_{AA}(f)$, $\hat{S}_{BB}(f)$ and $\hat{S}_{AB}(f)$ of $S_{AA}(f)$, $S_{BB}(f)$ and $S_{AB}(f)$ by:

$$\hat{S}_{AA}(f) = \frac{1}{n_d} \sum_{i=1}^{n_d} \hat{A}_i^{\star}(f) \cdot \hat{A}_i(f) \tag{9.1}$$

$$\hat{S}_{BB}(f) = \frac{1}{n_d} \sum_{i=1}^{n_d} \hat{B}_i^{\star}(f) \cdot \hat{B}_i(f) \tag{9.2}$$

$$\hat{S}_{AB}(f) = \frac{1}{n_d} \sum_{j=1}^{n_d} \hat{A}_j^*(f) \cdot \hat{B}_j(f) \tag{9.3}$$

From these two-sided spectral density estimates, the one-sided spectral density estimates $\hat{G}_{AA}(f)$, $\hat{G}_{BB}(f)$ and $\hat{G}_{AB}(f)$ are calculated according to (2.8) and (2.9) (Part I of the article, Section 2).

The errors can be divided into two types, bias errors $b[\hat{X}]$ and random errors $\sigma[\hat{X}]$, where $\hat{X}$ is the estimate of the true value X. A bias error $b[\hat{X}]$ is a systematic error introduced either in the measurement or in the analysis (post-processing). In some situations a bias error can be estimated either by performing certain measurements (of phase and gain differences in the two instrumentation channels for instance) or from theoretical calculations. The bias error can in such situations be corrected for, but this is not the case in general.

The random error $\sigma[\hat{X}]$ is the standard deviation of the estimates $\hat{X}$ and is due to the fact that averaging is not performed over an infinite number of records i.e. over infinitely long time, as shown in (2.4), (2.5) and (2.7). Averaging over the finite number of records n_d causes a random scatter in the estimates.

The bias error $b[\hat{X}]$ is defined by:

$$B[\hat{x}] = E[\hat{x}] - X \tag{9.4}$$

while the random error is defined as the standard deviation of $\hat{X}$ and therefore given by (see (3.3) in Section 3):

$$\sigma[\hat{X}] = \sqrt{E[(\hat{X} - E[\hat{X}])^2]} \tag{9.5}$$

$E[\ ]$ means "expected value of" and X is the true value.

Often it is more practical to work with the normalized errors instead of the absolute errors $b[\hat{X}]$ and $\sigma[X]$, The normalized bias error $\in_b$, and the normalized random (standard) error $\in_r$ gives the error as a fractional portion of the true value and are defined by:

$$\in_b = \frac{b[\hat{X}]}{X} \tag{9.6}$$

$$\in_r = \frac{\sigma[\hat{X}]}{X}$$
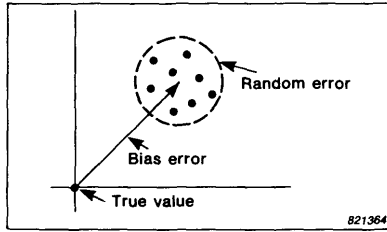
It is assumed that $X \neq 0$.

Fig. 52. Illustration of bias error and random error

Fig.52 gives an illustration of how a bias error and a random error influences the estimates of a value.

Bias errors in the different functions can be due to several effects such as

a) Extraneous noise at input and/or at output.
b) Other inputs to system which are correlated with measured input.
c) Leakage (resolution bias).
d) Non-linearities.
e) Propagation time delays not compensated for.

The effects of a), b) and c) were dealt with for the Frequency Response Function estimates in Section 4 and the influence of non-linearities were mentioned in Sections 3 and 5, and shall therefore not be discussed further here. If there is a propagation time delay τ from input to output of the system, this time delay has to be set between the records in the dual channel FFT measurement (see Fig.13 Section 3). Otherwise the Cross Spectrum will be biased with a factor of $(1 - {}^\tau/T)$, where T is the record length in the analysis. Thus

$$\hat{G}_{AB}(f) \approx (1 - {}^\tau/_T)\, G_{AB}(f) \quad , \quad 0 \le \tau \le T \qquad (9.8)$$

The functions derived from the Cross Spectrum will therefore also have a bias error.for example, the Coherence Function estimate is given by

$$\hat{\gamma}^2(f) \approx (1 - {}^\tau/_T)^2\, \gamma^2(f) \quad , \quad 0 \le \tau \le T \qquad (9.9)$$

The random errors will now be discussed for the Autospectral and Cross Spectral density estimates and for the estimates of Coherence Function and Frequency Response Functions. These formulae were developed by Bendat and Piersol (Ref. [23] and [24]). The random errors associated with the sound intensity measurements will also be given.

The distribution of the data is assumed to be Gaussian (normal). This is a fair assumption when the random error ϵ_r is small. The filtering (FFT analysis) also tends to make the distribution of the time data closer to the Gaussian distribution.

For Gaussian distributed estimates $\hat{X}$ (without any bias error ϵ_b) it can be shown that there is approximately 68% chance of the true value X to be within the interval,

$$\hat{X}\,(1 - \epsilon_r) \le X \le \hat{X}\,(1 + \epsilon_r) \tag{9.10}$$

and approximately 95% chance of the true value to be within the interval

$$\hat{X}\,(1 - 2\,\epsilon_r) \le X \le \hat{X}\,(1 + 2\,\epsilon_r) \tag{9.11}$$

9.1. Auto Spectral and Cross Spectral density estimates

If averaging is performed over n_d time records of the random signals $a(t)$ and $b(t)$, the normalized random (standard) error for a frequency component of the Autospectral density estimates $\hat{G}_{AA}(f)$ and $\hat{G}_{BB}(f)$ at any frequency is given by

$$\epsilon_r[\hat{G}_{AA}(f)] = \epsilon_r[\hat{G}_{BB}(f)] = \frac{1}{\sqrt{n_d}} \tag{9.12}$$

Notice that the random error is independent of frequency, n_d corresponds to the socalled BT-product (product of analysis bandwidth B and total effective time record length T_{Total}) for the analysis. If rectangular weighting is used in the analysis we have $B = \Delta f = {}^1/T$ and $T_{Total} = n_d\,T$,

giving $B \cdot T_{Total} = \frac{1}{T}\,n_d\,T = n_d$. T is the record length for each analysis.

If a smooth weighting function such as the Hanning weighting is used, the bandwidth B will be wider than Δf. The effective time length T_{eff} of each record will, however, be correspondingly shorter than T, due to the time weighting function. For each independent record, $B \cdot T_{eff}$ will be unity and therefore $B \cdot T_{Total} = B \cdot T_{eff} \cdot n_d = n_d$.

Since the effective time length is shorter than T when Hanning weighting is used, averaging of spectra estimates from time records having some overlap (50% or 75% overlap for instance) will allow for a higher BT-product i.e. a higher number n_d, compared to an analysis performed with rectangular weighting for a given amount of time data, see Ref. [16].

The magnitude $|\, G_{AB}(f)\,|$ of the Cross Spectral density $G_{AB}(f)$ will at any frequency be estimated with a normalized random error of

$$\epsilon_r \left[\, |\, \hat{G}_{AB}(f)\,|\, \right] = \frac{1}{\sqrt{\gamma^2(f)\, n_d}} \qquad (9.13)$$

where $\gamma^2(f)$ is the Coherence Function.

The lower the Coherence is in the measurement the more averaging is required in order to obtain a certain statistical accuracy in the estimate.

This is intuitively clear due to the fact that the lower the Coherence is the more random variation will there be in the individual estimates $\hat{A}^*_i(f) \cdot \hat{B}_i(f)$ (see Fig.4 and 9, Section 2 and 3).

9.2. Coherence Function estimates

The Coherence Function $\gamma^2(f)$ will also be estimated with only a limited accuracy from the Autospectral and Cross Spectral density estimates.

$$\hat{\gamma}^2(f) = \frac{|\, \hat{G}_{AB}(f)\,|^2}{\hat{G}_{AA}(f)\quad \hat{G}_{BB}(f)} \qquad (9.14)$$
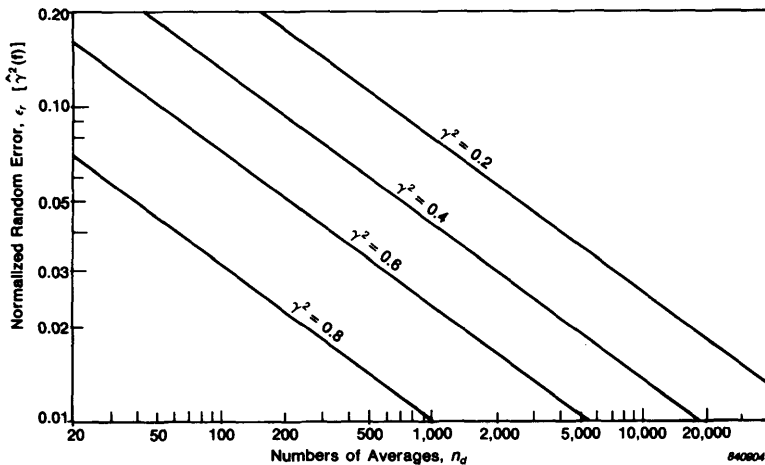
Fig. 53. Normalized random error $\in_r[\gamma^2(f)]$ of Coherence Function esti-
mates as a function of number of averages n_d, for different
values of (true) Coherence $\gamma^2(f)$

39

The normalized random (standard) error is given by

$$\epsilon_r\left[\ \hat{\gamma}^2(f)\ \right] = \frac{\sqrt{2}\ (1-\gamma^2(f)\ )}{\sqrt{\gamma^2(f)\ n_d}} \tag{9.15}$$

If the number of averages $n_d = 1$, we have that

$$\hat{\gamma}^2(f) = \frac{|\ \hat{A}_i^*(f)\ \hat{B}_i(f)\ |^2}{|\ \hat{A}_i(f)\ |^2\ |\ \hat{B}_i(f)\ |^2} = \frac{\hat{A}_i^*(f)\ \hat{A}_i(f)\ \hat{B}_i^*(f)\ \hat{B}_i(f)}{\hat{A}_i^*(f)\ \hat{A}_i(f)\ \hat{B}_i^*(f)\ \hat{B}_i(f)} = 1$$

Some averaging will therefore always have to be performed in order to estimate the Coherence Function. Even if the Coherence is unity, averaging is required to verify this in a measurement.

Fig.53 shows the relationship between the normalized random error $\epsilon_r\ [\gamma^2(f)]$ and the number of averages n_d for different values of (true) Coherence $\gamma^2(f)$.

9.3. Frequency Response Function Estimates

When the Frequency Response Function of an ideal system is estimated from $H_1(f)$ or $H_2(f)$ and the signals are random noise signals (bandwidth-limited, Qaussian distributed white noise signals) there is a random error in both magnitude and phase. The error depends upon the number of (independent) averages n_d and the Coherence $\gamma^2(f)$ in the measurement.

The normalized random error for the magnitude of the estimate $|H(f)|$ ($|H_1(f)|$ or $|H_2(f)|$) is given by

$$\epsilon_r\left[\ |\hat{H}(f)|\ \right] = \sqrt{\frac{1-\gamma^2(f)}{\gamma^2(f)\ 2\ n_d}} \tag{9.16}$$

In Fig.54 the normalized random error $\epsilon_r\ [|H(f)|]$ is plotted as a function of number of averages n_d for different values of Coherence $\gamma^2\{f\}$. The more uncorrelated noise there is in the measurement i.e. the lower the Coherence is, the more averages have to be performed in order to get a certain statistical accuracy.

Fig.55 shows the estimates of $|H_1(f)|$ and $\gamma^2(f)$ from a dual channel measurement on an electrical filter network with random noise excita-

tion. 100 averages are performed. The estimated Coherence $\hat{\gamma}^2(f)$ at 176 Hz is 0,6, due to uncorrelated noise at the output. The random error of $\hat{\gamma}^2(f)$ is

$$\epsilon_r\left[\ \hat{\gamma}^2(f)\ \right] \simeq \frac{\sqrt{2}\cdot 0,4}{\sqrt{0,6\cdot 100}} \approx 0,07.$$

The random error for $|H_1(f)|$ at the same frequency is

$$\epsilon_r\left[\ |\ \hat{H}_1(f)\ |\ \right] \simeq \sqrt{\frac{0,4}{0,6\cdot 200}} \approx 0,06$$

which in dB is $\approx$ 0,5dB.

Thus there is 68% chance of the true value $|H_1(f)|$ at 176 Hz, to be within the interval (since we have no bias error, see Section 4.2)

$0,94 \cdot |\hat{H}_1(f)| \leq |H_1(f)| \leq 1,06\ |\hat{H}_1(f)|$
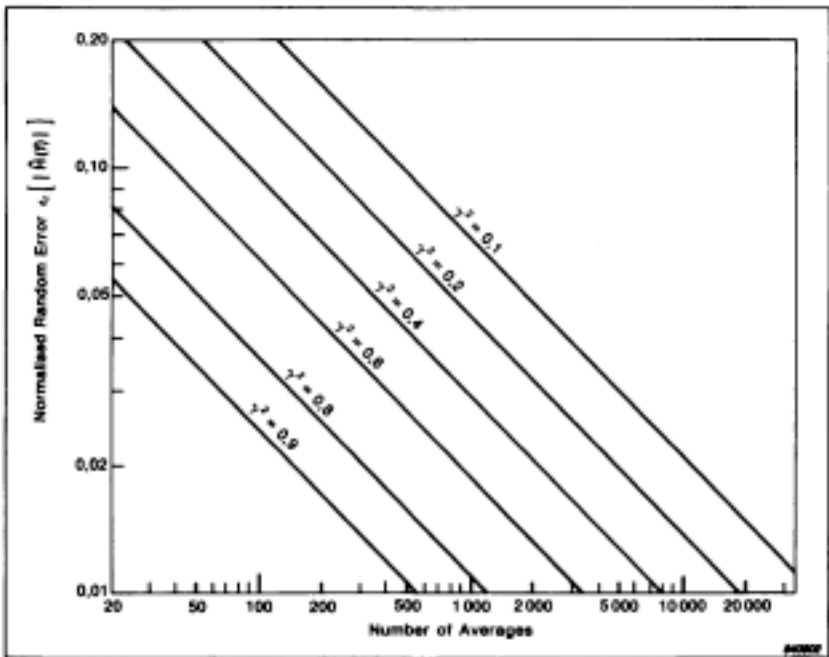
Fig. 54 Normalized random error $\in_r$ [$|\hat{H}_1(f)|$] of magnitude of Frequency Response Function estimates ($\hat{H}_1(f)$ or $\hat{H}_2(f)$) as a function of number of averages nd for different values of Coherence $\gamma^2(f)$
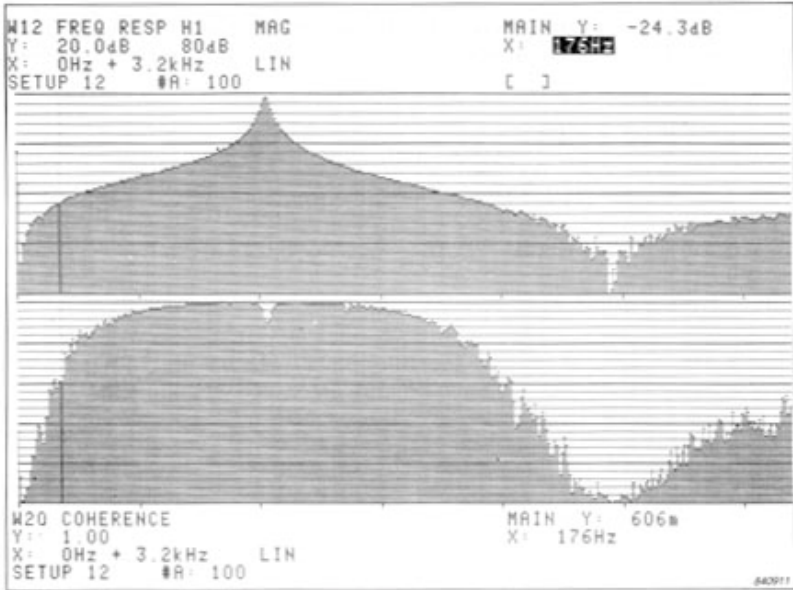
Fig. 55. Estimates of $|H_1(f)|$ and γ^2 from a dual channel measurement on an electrical filter network, with random noise excitation and 100 averages

or in dB

$$-24,8 \quad \text{dB} \quad \leq \quad |H_1(f)| \quad \text{(dB)} \quad \leq \quad -23,8 \quad \text{dB} \quad \text{since} \quad |H_1(f)| \quad = \quad -24,3 \quad \text{dB.}$$

The random errors at the same frequency for the Autospectra $G_{AA}(f)$ and $G_{BB}(f)$ and the magnitude of the Cross Spectrum $|G_{AB}(f)|$, which are used for the calculations, are

$$\epsilon_r\left[\,|\hat{G}_{AA}(f)|\,\right] = \epsilon_r\left[\,|\hat{G}_{BB}(f)|\,\right] = \frac{1}{\sqrt{100}} = 0,10$$

and
$$\epsilon_r\left[\,|\hat{G}_{AB}(f)|\,\right] \simeq \frac{1}{\sqrt{0,6 \cdot 100}} \approx 0,13$$

Notice that these random errors are greater than the errors on the derived functions $\gamma^2(f)$ and $|H_1(f)|$.

The random error for the phase angle $\phi(f)$ of $H(f)$ can be approximated by

42

$$\sigma\,[\phi\,(f)] \approx \epsilon_r\,[\,|H(f)\,|\,] \qquad\qquad (9.17)$$

when the error $\epsilon_r\,[\,|H(f)\,|\,]$ is small. $\Phi(f)$ is measured in radians. The true value $H(f)$ is here assumed, with 68% confidence, to be inside a circle of radius $\sigma\,[\,|H(f)\,|\,]$ and centered at $H(f)$. Thus

$$\sigma\,[\Phi(f)] \approx \sin\,(\sigma\,[\Phi(f)]) \approx \frac{\sigma\,[\,|H(f)\,|\,]}{|H(f)\,|}$$

giving equation (9.17), for small $\sigma\,[\Phi(f)]$ or $\epsilon_r\,[\,|H(f)\,|\,]$.

9.4 Sound Intensity

The sound intensity I_r (component in the direction of the probe) in a random sound field is as the other functions, estimated with a limited statistical accuracy. The bias error basically depends on the spacing between the microphones (high frequencies) and on the residual phase mismatch between the two channels in the measurement system (low frequencies). This is described in the references.

The random error is determined by the Coherence Function $\gamma^2(f)$ between the two sound pressure signals $p_A(t)$ and $p_B(t)$, the phase angle ϕ_{AB} of the Cross Spectrum $G_{AB}(f)$ between the two signals and the number of averages n_d. In Ref. [25] a formula for the normalized random error $\epsilon_r\,[\,\hat{I}_r\,]$ is derived

$$\epsilon_r\,\left[\,\hat{I}_r\,\right] = \frac{1}{\sqrt{n_d}}\,\sqrt{\frac{1}{\gamma^2(f)} + \cot^2\left(\phi_{AB}(f)\right)\frac{1-\gamma^2(f)}{2\,\gamma^2(f)}} \qquad (9.18)$$

Calculations of Coherence $\gamma^2(f)$ and phase angle $\phi_{AB}(f)$ in different situations are givep in Ref. [26]. These calculations indicate that the random error $\epsilon_r\,[\hat{I}_r]$ mainly depends upon the reactivity L_K of the sound field, defined as the difference between sound intensity level L_I and sound pressure level L_p, and also depends upon the interfering sound field in the different situations (diffuse background noise or an interfering point source either perpendicular to or behind the probe, which points towards the source of interest). The random error, however, was found to be practically independent of the frequency and distance between the microphones.

It is therefore very important to check and report the reactivity of the sound field where the intensity measurements are performed, in order to be able to judge the validity of the results.

References

[12] THRANE, N.   "The Hilbert Transform", B & K *Technical Review,* No.3 - 1984.

[13] BIERING H. &
    PEDERSEN, O.Z.   "System Analysis and Time Delay Spectrometry", B&K *Technical Review,* No.1 and 2, 1983

[14] RANDALL, R. B. &
    HEE, J.   "Cepstrum Analysis", B & K *Technical Review,* No.3, 1981.

[15] GADE,S.   "Sound Intensity", B&K *Technical Review,* No.3 and 4, 1982.

[16] THRANE, N.   "Zoom FFT", B&K *Technical Review,* No.2, 1980.

[17] FAHY, F.J.   "Measurement of Acoustic Intensity Using the Cross Spectral Density of two microphone signals.", Journal of the Acoustical Society of America 62(4) 1057-1059, 1977.

[18] CHUNG, J.Y.   "Fundamental Aspects of the Cross Spectrum method of measuring Acoustic Intensity". Senlis, 1981, pp.1-10.

[19] CHUNQ, J.Y. &
    POPE, J.   "Practical measurement of Acoustic Intensity - the two microphone cross spectral method" *Proc. Internoise* 1978, pp.893-900.

[20] GADE, S.,et al: "Sound Power determination using Sound Intensity measurements" (Part I and II) B&K Appl. Notes.

[21] CROCKER, M.J.et al.   "Application of Acoustic Intensity Measurements for the evaluation of Transmission loss of structures" Senlis 1981, pp.161-169.

[22] QINN, K.B.et.al.   "Sound Power determination in highly re-active environments using sound intensi-ty measurements", B&K Application Notes.

[23] BENDAT, J.S. & PIERSOL, A. G.   "Random Data: Analysis and Measure-ment Procedures", Wiley-Interscience, 1971.

[24] BENDAT, J.S. & PIERSOL, A. G.   "Engineering Applications of Correlation and Spectral Analysis", John Wiley & Sons, 1980.

[25] SEYBERT, A. F.   "Statistical Errors in Acoustic Intensity Measurements", Journal of Sound and Vibration, 1981, 75, pp.519-526.

[26] DYRLUND, O.   "A note on Statistical Errors in Acoustic Intensity Measurements.", Letters to the Editor, *Journal of Sound and Vibration,* 1983. 90, pp.585-589.

[27] NICOLAS, J., BENQIT, R., SAUVE, S.   "Noise source identification and reduc-tion in a chocolate plant", *Proceedings of Noise-Con.* '83.

[28] YANO, H., TACHIBANA, H., ISHII, K.   "Application of sound intensity measur-ing technique to sound insulation mea-surements", *ICA* 1983.

[29] RASMUSSEN, G., RASMUSSEN,P.   "Identification of energy sources and ab-sorbers", *Proceedings of the 2nd Inter-national Modal Analysis Conference,* 1984.

[30] COLEMAN, R.B., HODGSON.T.H.   "Acoustic Intensity Measurements on a 350 kN Automatic Punch Press", *Pro-ceedings of Inter-Noise'83.*

News from the Factory

Dual Channel Signal Analyzers Type 2032/2034
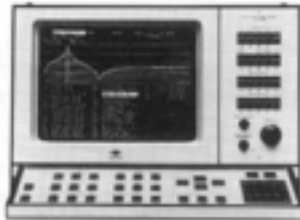
The Analyzers Type 2032 and Type 2034 combine the use of realtime, digital filtering techniques with a 2 k (2048 points) Fourier Analysis in two channels. Thus 801-line spectra are calculated with a chosen resolution from 1,95 mHz to 32 Hz selected in binary steps anywhere in the frequency range from DC to 25,6kHz.

Both analyzers are extremely fast. The standard version, Type 2034, has a real-time bandwidth of 1,6 kHz in single channel mode and 800 Hz in dual channel mode. The high speed version, Type 2032, is approximately six times faster.

34 different functions are available such as Frequency Response, Impulse Response, Autospectra, Cross Spectrum, Correlation Functions, Enhanced Signals and their spectra, Distribution Functions, Coherence, Coherent Power, Sound Intensity, Cepstra, etc., etc. Most of these functions, including time domain functions, can be shown in 6 different formats: Real Part, Imaginary Part, Magnitude, Phase, Nyquist Plot and Nichols Plot. Two micro-processors are used in carrying out all the calculations: One for signal processing and the other for displaying (postprocessing) the data. Thus any function can be displayed at any time in any format and scaling, not only after a measurement has been completed, but also during a measurement.

The primary use of a dual channel analyzer is for system analysis, i.e. performing Frequency Response (and Impulse Response) measurements. Two different ways of calculating the Frequency Response Function are implemented in the 2032/2034: The traditional way $H_1 = G_{AB}/G_{AA}$ and the new way $H_2 = G_{BB}/G_{BA}$. H_1 suppresses uncorrelated noise at the output and gives the best estimate at anti-resonances. H_2 suppresses uncorrelated noise at the input and gives the best estimate at the resonance peaks.

The analyzers are equipped with extremely flexible trigger facilities.

A Free Running, Internal, External or manual trigger source can be selected in addition to a Generator trigger, where data collection is synchronized to the sequence of the built-in, zooming pseudo-random or impulse generator. Zooming random noise and a sine signal with a selectable frequency are also available.

Each channel can be independently set to have a Flat, Manning, Transient, Exponential, Flat Top, Kaiser Bessel or User Defined weighting function. These weighting functions can even be applied to the Frequency Response Function, Cross Spectrum and Autospectra before calculating the Impulse Response, Cross Correlation and Autocorrelation Functions.

The analyzers have seven cursor functions. Namely, Main Cursor, Harmonic Cursor, Sideband Cursor, Delta Cursor, Mask Cursor, Reference Cursor and even a Flex Cursor by which the x-axis can be scaled in any arbitrarily chosen engineering unit.

In spite of the high level of complexity and sophistication, the analyzers are very easy to use, because operation is largely self-explanatory with all relevant control settings clearly shown on its display screen, and because complete measurement and display setups can be stored for later recall and use.

The analyzers have a fully instrumented front end, by which they can accept signals from most B&K microphone preamplifiers, and via the Line Drive Amplifier Type 2644 from most accelerometers, force transducers and the Impact Hammer Type 8202 in either of its channels. In addition, the 2032/2034 are equipped with DC-coupled direct inputs for the input of electrical signals.

Output of the data which is displayed on a 12-inch large raster screen can be made to an X-Y recorder, a video recorder or to the B&K Graphics Recorder Type 2313, where a complete copy of the screen including graphs and alphanumerics are made in less than 10 seconds. The 2032/2034 are also equipped with an extremely flexible and sophisticated IEC 625-1/IEEE Std. 488-1978/ANSI MC 1.1-1975 interface which allows simple connection to most desk-top calculators.

Graphics Recorder Type 2313
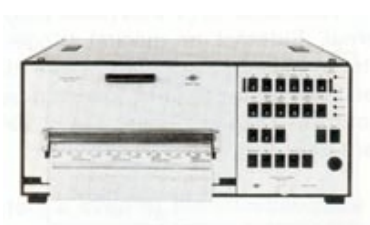
The Brüel & Kjær Graphics Recorder Type 2313 offers fast, fully annotated, graphic plots of measured frequency spectra and time functions as presented on the display screen of B&K Digital Frequency Analyzers, as well as documents measurement data transmitted by other equipment furnished with an IEC/IEEE interface.

For maximum operating flexibility, a range of interchangeable Application Packages is available. These plug-in the front of the 2313 and especially format data to suit different application requirements of B&K analyzing equipment. In addition, they permit a variety of special tasks to be carried for which extra equipment would normally be required. For example, several hundred complete measurement spectra can be stored in the Recorder for future print out or transmission to other equipment. Also, new types of measurement can be made using the 2313 to reformat stored and incoming data, plus use as a system controller is possible.

Where use as a conventional alphanumeric printer/graphics recorder is concerned, the 2313 may be operated without an Application Package. High-resolution graphic plots are made using a 512-point print head and as many as 128 (ISO 646 and 2022) characters may be printed. It accepts 50m rolls of electrosensitive paper (metallized type) and from just one roll the equivalent of 160 A 4 charts can be obtained.

PREVIOUSLY ISSUED NUMBERS OF
BRÜEL & KJÆR TECHNICAL REVIEW

(Continued from cover page 2)

SPECIAL TECHNICAL LITERATURE

As shown on the back cover page, Brüel & Kjær publish a variety of technical literature which can be obtained from your local B & K representative.

The following literature is presently available:

Mechanical Vibration and Shock Measurements
(English), 2nd edition
Acoustic Noise Measurements (English), 3rd edition
Architectural Acoustics (English)
Strain Measurements (English, German)
Frequency Analysis (English)
Electroacoustic Measurements (English, German, French, Spanish)
Catalogs (several languages)
Product Data Sheets (English, German, French, Russian)

Furthermore, back copies of the Technical Review can be supplied as shown in the list above. Older issues may be obtained provided they are still in stock.

BV 0014-11

Brüel & Kjær